The Astrophysical Journal, 862:106 (28pp), 2018 August 1 https://doi.org/10.3847/1538-4357/aacb7a


# Characterization of Stellar and Substellar Members in the Coma Berenices Star Cluster

Shih-Yun Tang[1], W. P. Chen[1,2], P. S. Chiang[2], Jessy Jose[3,4], Gregory J. Herczeg[3], and Bertrand Goldman[5,6]
[1] Department of Physics, National Central University, 300 Zhongda Road, Zhongli, Taoyuan 32001, Taiwan
[2] Graduate Institute of Astronomy, National Central University, 300 Zhongda Road, Zhongli, Taoyuan 32001, Taiwan
[3] Kavli Institute for Astronomy and Astrophysics, Peking University, Yi He Yuan Lu 5, Haidian District, Beijing 100871, People's Republic of China
[4] Department of Physics, Indian Institute of Science Education and Research, Rami Reddy Nagar, Karakambadi Road, Mangalam (P.O.) Tirupati 517507, India
[5] Max Planck Institute for Astronomy, Konigstuhl 17, D-69117 Heidelberg, Germany
[6] Universite de Strasbourg, CNRS, Observatoire astronomique de Strasbourg, UMR 7550, F-67000 Strasbourg, France
*Received 2018 March 7; revised 2018 June 4; accepted 2018 June 4; published 2018 July 27*

## Abstract

We have identified stellar and substellar members in the nearby star cluster Coma Berenices, using photometry, proper motions, and distances of a combination of 2MASS, UKIDSS, URAT1, and *Gaia*/DR2 data. Those with *Gaia*/DR2 parallax measurements provide the most reliable sample to constrain the distance, averaging 86.7 pc with a dispersion of 7.1 pc, and age of ∼800 Myr, of the cluster. This age is older than the 400–600 Myr commonly adopted in the literature. Our analysis, complete within 5° of the cluster radius, leads to identification of 192 candidates, among which, after field contamination is considered, about 148 are true members. The members have $J \sim 3$ mag to ∼17.5 mag, corresponding to stellar masses 2.3–0.06 $M_\odot$. The mass function of the cluster peaks around 0.3 $M_\odot$, and in the sense of $dN/dm = m^{-\alpha}$, where $N$ is the number of members and $m$ is stellar mass, with a slope $\alpha \approx 0.49 \pm 0.03$ in the mass range 0.3–2.3 $M_\odot$. This is much shallower than that of the field population in the solar neighborhood. The slope $\alpha = -1.69 \pm 0.14$ from 0.3 $M_\odot$ to 0.06 $M_\odot$, the lowest mass in our sample. The cluster is mass-segregated and has a shape elongated toward the Galactic plane. Our list contains nine substellar members, including three new discoveries of an M8, an L1, and an L4 brown dwarfs, extending from the previously known coolest members of late-M types to even cooler types.

*Key words:* brown dwarfs – stars: evolution – stars: luminosity function, mass function – open clusters and associations: individual (Coma)

*Supporting material:* machine-readable table

## 1. Introduction

Stars are formed in groups out of interstellar molecular clouds. Those clusters that remain gravitationally bound, i.e., surviving internal dynamics and external disturbances, appear as star clusters. Stellar aggregates provide the early evolutionary environments for a star, in which planets and moons are formed. Since members in a star cluster are formed essentially at the same time, and share similar compositions, space motions, and spatial locations in space, star clusters have been used extensively for studies of stellar evolution, tests, and calibrations of stellar atmospheric models, clustered star formation, starburst processes, or stellar dynamics (Brandner et al. 2008; Rochau et al. 2010; Gennaro et al. 2011).

An embedded or infrared cluster may not remain gravitationally bound as the turbulent parental cloud disperses (Lada & Lada 2003). Later on, through mutual gravitational interaction, higher-mass members lose kinetic energy and sink to the center, whereas lower-mass members gain speed and occupy a progressively larger volume of space. Those that exceed the escape velocity of the system, notably the least massive members at the time, are most susceptible to being thrown out ("stellar evaporation") to supply field stars (e.g., Mathieu 1984), with an evaporation timescale $\tau_{\rm evap} \approx 100(D/v)(0.1N/\ln N)$ for a system of $N$ equal-mass stars of a size scale $D$ and typical velocity $v$ (Shu 1982; Binney & Tremaine 1987; Bhattacharya et al. 2017).

It is not clear if there is an "initial mass function" for star clusters, namely, if more massive systems are favored or less preferred in formation. It is plausible that most star clusters we witness now are remnants of massive systems such as those super star clusters seen near the Galactic center (e.g., Brandner et al. 2008), the Orion Nebular cluster (e.g., Hillenbrand 1997), and the pristine globular clusters. In addition to internal stellar dynamics, Galactic disturbances also act to disintegrate a star cluster, with effects such as tidal disruption from nearby giant molecular clouds or star clusters, passages through spiral arms or disks, or shear forces arising from Galactic differential rotation. While the youngest systems are shaped by the parental cloud structure (Chen et al. 2004), tidal distortion is evidenced in many open clusters or even in globular clusters (Chen et al. 2004; Chen & Chen 2010; Bhattacharya et al. 2017). Only a recently dissolved star cluster in the solar neighborhood may be recognized as a star moving group, if the then-members still share common space positions and kinematics (Zuckerman & Song 2004).

While low-mass stars are susceptible to ejection, their total mass plays a decisive role in the survival of a star cluster (de Grijs & Parmentier 2007); a cluster must have a sufficient number of low-mass stars to have longevity ($\gtrsim$1 Gyr) against external stirring (de Grijs 2009). Nearby young systems such as Hyades (∼47 pc, 625 Myr), Praesepe (∼170 pc, 757 Myr; Gáspár et al. 2009; van Leeuwen 2009), and the Coma Berenices star cluster (∼90 pc, 600 Myr; Tsvetkov 1989; van Leeuwen 1999) are particularly suitable targets to identify the low-mass stellar or even substellar members in the context of cluster disintegration.

The Coma Berenices star cluster (Melotte 111, hereafter Coma Ber, R.A. = $12^{\rm h}25^{\rm m}$, decl. = 26°06′, J2000) was first listed by Melotte (1915), and Trumpler (1938) first characterized its stellar members. Despite its proximity, the cluster has been relatively poorly studied due to its large sky coverage ($>5°$), hence the difficulty in distinguishing members against field stars. Casewell et al. (2006) combined 2MASS (Two Micron All Sky Survey) and USNO-B1.0 (United States Naval Observatory) data to identify some 100 possible cluster members. Using optical and 2MASS photometric data, Melnikov & Eislöffel (2012) identified very-low-mass candidates to the limit of $I < 20.1$ mag in an area of 22.5 $\deg^2$, with no proper motion constraints except removal of high proper motion stars. Five of their candidates have luminosities and colors consistent with being brown dwarfs. Terrien et al. (2014) included SDSS/APOGEE (Sloan Digital Sky Survey, Apache Point Observatory Galactic Evolution Experiment) radial velocity data in membership determination, and found a few K and early-M members that were previously unknown.

Kraus & Hillenbrand (2007) conducted a comparative study between Praesepe and Coma Ber, using the 2MASS, SDSS, USNOB1.0, and UCAC-2.0 (USNO CCD Astrograph Catalog) surveys for photometric and astrometric member selection. They found a clear mass segregation in Praesepe, i.e., with massive stars being concentrated toward the central region, whereas lower-mass members occupied a progressively larger volume in space, but not in Coma Ber, which has a similar linear size but was thought to be somewhat younger. Wang et al. (2014) confirmed the mass segregation in Praesepe, and concluded that the lowest-mass members they detected, $\sim 0.1\ M_\odot$, are being stripped away.

Here, we present a comprehensive characterization of the stellar and substellar member candidates of Coma Ber. We first summarize the archival data on photometry, astrometry, and distance used in this work, and then report how membership is determined. A set of bright candidates with parallax distances serves as the high-confidence sample to constrain the cluster parameters, such as the distance, age, and size, etc., which in turn guide the identification of faint stellar and substellar candidates. We then present the infrared spectroscopy that confirm the brown dwarf nature of these members. With a sample of stellar and substellar members, we derive the luminosity function, mass function, shape, and dynamical status of the cluster. For a star with no parallax measurement available, we derive the distance by first estimating its spectral type from photometric colors, and then comparing the observed flux to the expected luminosity for that spectral type. We describe the method in the Appendix.

## 2. Data and Analysis

In this work, stellar membership is diagnosed by grouping of stars in position in space and in kinematics. For bright stars, we use 2MASS photometry and URAT1 (USNO Robotic Astrometric Telescope) proper motions, whereas for faint stars, we analyze both the photometry and proper motions from the UKIRT Infrared Deep Sky Survey (UKIDSS) and Galactic Clusters Survey (GCS, Lawrence et al. 2012). Distance information comes from parallax measurements by *Gaia*/DR2, or is estimated using the spectral type.

### 2.1. Archival Data for Distance

Distance determination is based on parallax measurements, whenever available, by *Gaia*/DR2 (Gaia Collaboration et al. 2018). *Gaia* is a space mission designed for astrometry by the European Space Agency, launched on 2013 December 19. The latest data release (DR2), including the first 22 months of the nominal mission lifetime, contains celestial positions and apparent brightness for ~1.7 billion sources, among which 1.3 billion also have parallaxes and proper motions available (Lindegren et al. 2018). For our study the empirical limit for the *Gaia*/DR2 is $J \sim 15$ mag, and only measurements with $\varpi/\Delta\varpi > 10$ are considered in the analysis, where $\varpi$ is the parallax and $\Delta\varpi$ is the error (Lindegren et al. 2018).

For an object with no parallax data, we estimate its spectral type via multiband photometry, from which the distance is derived. Photometric data in optical wavelengths include those of SDSS/DR12 (Alam et al. 2015) and PS1 (Panoramic Survey Telescope and Rapid Response System, Chambers et al. 2016). In a few cases we utilize the SDSS flags to distinguish a star from a galaxy. For photometry extending to mid-infrared wavelengths, "ALLWISE" (Cutri et al. 2013) has been used, which combines the data of the *Wide-field Infrared Survey Explorer* (*WISE*) (Wright et al. 2010) in the cryogenic phase of the mission, and NEOWISE (Mainzer et al. 2011) in the first post-cryogenic phase.

### 2.2. Archival Data for Proper Motion and Photometry

Proper motions are taken from *Gaia*/DR2 when available, as long as the measurements are reliable, again with $\varpi/\Delta\varpi > 10$. Alternatively, proper motions are extracted from URAT1 (Zacharias et al. 2015), which is an astrometric catalog as a follow-up project of UCAC. In addition to proper motions, with typical errors 5–8 mas $\mathrm{yr}^{-1}$, URAT1 provides photometry in one single "*f*" band (between *R* and *I*). URAT1 covers almost the entire northern sky and extends down to decl. $-15°$ in some areas, cataloging over 228 million objects at a mean epoch around 2013 May. A large fraction (83%) of the URAT1 entries ($3''$ matching radius) list 2MASS *J*, *H*, and $K_s$ magnitudes. Some 16% of URAT1 sources are supplemented with five-band photometry (BVgri) from the AAVSO Photometric All-Sky Survey (APASS).

In our analysis, photometry is taken from 2MASS whenever available. The 2MASS Point Source Catalog (Skrutskie et al. 2006) has $10\sigma$ detection limits of $J \sim 15.8$ mag, $H \sim 15.1$ mag, and $K_s \sim 14.3$ mag, and saturates around $J \sim 9$ mag, $H \sim 8.5$ mag, and $K_s \sim 8$ mag.

The UKIDSS/GCS aimed to measure the very-low-mass end of the stellar mass functions in 10 star clusters. As for other UKIDSS surveys, the Large Area Survey (LAS) covered only the edge of Coma Ber, whereas the Galactic Plane Survey (GPS) did not include Coma Ber at all. Proper motions are available for UKIDSS/GCS starting with DR9 (Collins & Hambly 2012; Smith et al. 2014). For the work reported here, we use the latest data release DR10, but its spatial coverage is incomplete within the surveyed sky of 78.5 $\deg^2$ toward the cluster (see Figure 1), missing a sky area of about 7 $\deg^2$ in the *Z*- and *Y*-bands, 2.5 $\deg^2$ in the *J*-band, and 3 $\deg^2$ in the *H*-band, due to poor data quality (Boudreault et al. 2012). The *K*-band observations were taken at 2 epochs to enable proper motion estimates. The typical proper motion error of the GCS in our data is about 5 milli-arcseconds (mas) per year. We have made use of the *ZYJHK* data, with the detection limits at an error of 0.15 mag $Z = 20.5$, $Y = 20.3$, $J = 19.5$, $H = 18.8$, $K1 = 18.0$, and $K2 = 18.1$ mag, respectively, and with the saturation limits $Z = 11.3$, $Y = 11.5$, $J = 11.0$, $H = 11.3$, and $K1 = 9.9$ mag (Lodieu et al. 2012). The photometric sensitivity of each band is depicted in Figure 2.

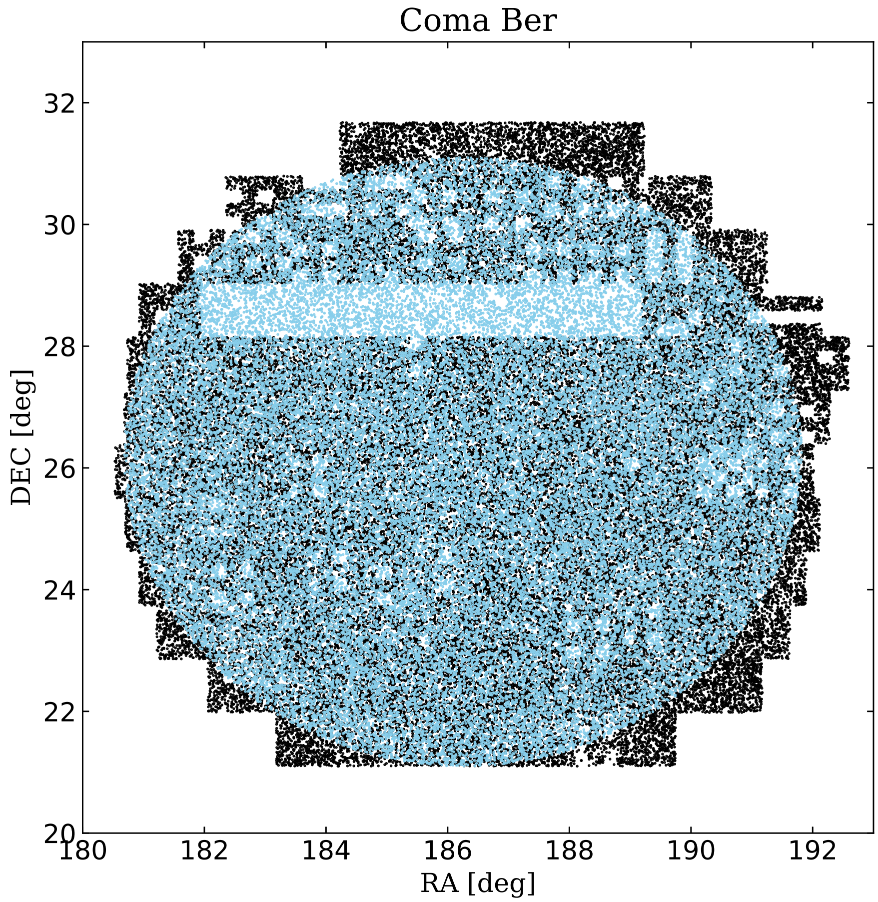


**Figure 1.** UKIDSS/GCS sources (in black) toward Coma Ber with *ZYJKs* photometric measurements. No data are available in the blank regions due to poor image quality flagged by the UKIDSS quality control. Also shown are the 2MASS sources (in light blue) within the 5° radius of the "cluster region" of our study. For display clarity, only one in two sources, selected randomly, is shown.

Our investigation is limited to UKIDSS sources with a probability greater than 70% of being a star, using the UKIDSS database flag to distinguish a star from a galaxy, with a photometric error less than 0.15 mag and being fainter than $J = 12$ mag. The sky area of our study, limited by the UKIDSS/GCS coverage of 78.5 deg$^2$, or about a 5° radius toward Coma Ber, is chosen as the "cluster region." In addition, a patch of sky of a 3° radius roughly 11° to the east from the cluster center is used in experimental design as the "control field."

## 3. Members of the Coma Ber Star Cluster

The early work by Trumpler (1938) led to the identification of 37 members brighter than a photographic magnitude of 10.5 within a 7° diameter on the basis of proper motions, color–magnitude relation, and radial velocities. An additional seven candidates with no radial velocity measurements were also proposed. While the bright members in Coma Ber display a density structure similar to those of Praesepe and the Pleiades (Artyukhina & Kholopov 1966), there is a paucity of faint members, often attributed to stellar evaporation (Argue & Kenworthy 1969). Candidates reported recently by Casewell et al. (2006, 105 members), Kraus & Hillenbrand (2007, 149 members), and Mermilliod et al. (2008, 31 members) are mostly bright. The later work by Melnikov & Eislöffel (2012, 82 stars) expanded the member list to include late-M spectral types, i.e., into the brown dwarf regime. The selection by Mermilliod et al. (2008) included radial velocities for some candidates, but neither Mermilliod et al. (2008) nor Melnikov & Eislöffel (2012) incorporated proper motion information into membership determination.

The age of Coma Ber reported in the literature ranges from ∼300 Myr to 1 Gyr (Tsvetkov 1989, summarized in their Table 5), but usually an age between 400 Myr and 600 Myr is adopted (Odenkirchen et al. 1998; Kraus & Hillenbrand 2007; Casewell et al. 2014).

### 3.1. Evolved Members

We analyze evolved members to constrain the age. In Coma Ber, any post-main-sequence members are too bright to render reliable 2MASS photometry, so we characterize them with optical photometry. Table 1 lists the parameters of the five brightest stars in the region. For 18 Com, a subdwarf F5 IV with a *Gaia* distance 59.8 ± 0.4 pc and proper motions $(\mu_\alpha \cos\delta, \mu_\delta) = (-17.57 \pm 0.17, 0.68 \pm 0.12)$ mas yr$^{-1}$,[7] its deviation from theoretical isochrones (shown in Figure 3) suggests that it is not a part of the cluster. The other four stars have distance, photometry, and kinematics consistent with membership. The star 12 Com, a known member, is a double-lined spectroscopic binary (Griffin & Griffin 2011) consisting of an A2/A3 dwarf and a mid-typed giant (Abt (2008, F6 III),

[7] Note URAT1 gives very different proper motions, $(\mu_\alpha \cos\delta, \mu_\delta) = (-12.0, 9.3)$ mas yr$^{-1}$, with an error of 5.9 mas yr$^{-1}$ in both axes.

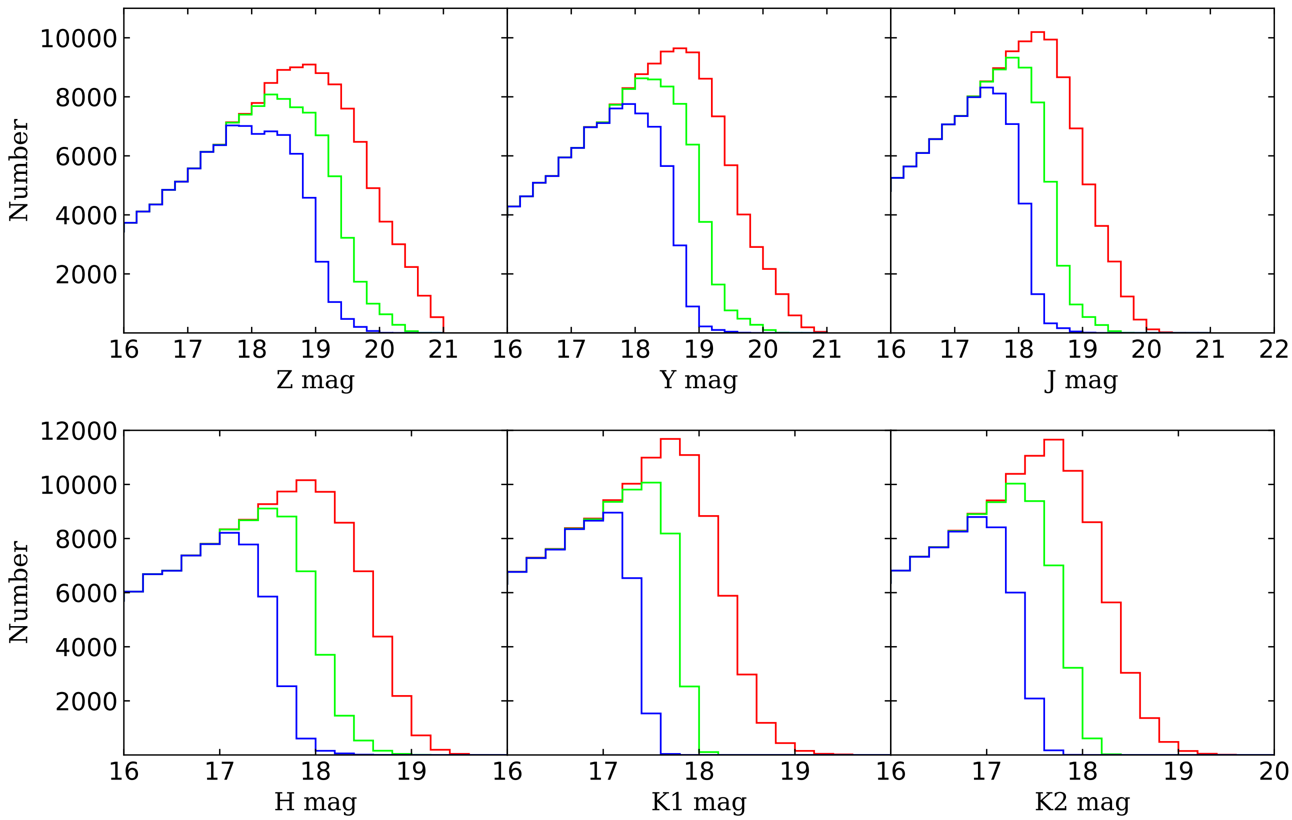


**Figure 2.** Number of UKIDSS/GCS stars in various bands, for all the stars (the red line) in the cluster region shown in Figure 1, and for those with photometric errors less than 0.15 mag (green) or 0.10 mag (blue).

Griffin & Griffin (1986, G7 III)). The coeval age of the binary system 670 Myr (Griffin & Griffin 1986) and a *Gaia* distance 84.5 ± 1.7 pc both indicate membership.

The star 31 Com, a G0 IIIp giant, known to have varying $v \sin i$ (Massarotti et al. 2008), suggestive of binarity, is located at 6.8 deg from the cluster center, i.e., outside our analysis range, but it has photometry, astrometry, and distance consistent with membership. It has been considered a member by Casewell et al. (2006) and by Mermilliod et al. (2008), and is also included in our member list.

Using the Padova isochrone (Bressan et al. 2012), assuming null reddening ($E(B - V) = 0.006$, Nicolet 1981) and solar metallicity (Friel & Boesgaard 1992; Netopil et al. 2016), an age of 800 Myr gives an overall better fit than younger ages, as evidenced in Figure 3, where for each star the absolute magnitude is computed using the *Gaia*/DR2 parallax and the apparent magnitude taken from the Bright Star Catalog, without correction for extinction or reddening. The fit is considered satisfactory, given the known binarity of 12 Com and 31 Com, and non-membership of 18 Com. We therefore conclude Coma Ber to be about 800 Myr old.

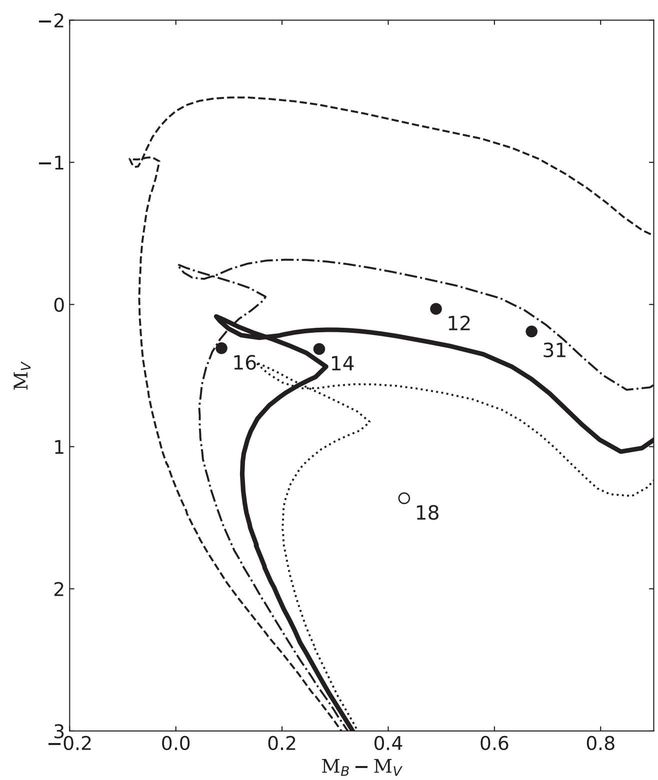


**Figure 3.** Optical absolute $M_V$ vs. $M_B$–$M_V$ diagram for the brightest stars in the cluster region. Each number labels the name of a star, e.g., “12” means 12 Com in Table 1. Also plotted are the PARSEC isochrones, from top to bottom, of 300 Myr, 600 Myr, 800 Myr (thick line), and 1000 Myr. An age of 800 Myr fits the data better than younger ages.

### *3.2. Bright Members*

A bright candidate is selected as having proper motions, from *Gaia*/DR2 or from URAT1, within 17 mas yr$^{-1}$ from $(\mu_\alpha \cos\delta, \mu_\delta) = (-11.21, -9.16)$ mas yr$^{-1}$, a range judiciously chosen to include all known proper motion members in the literature. Figure 4 illustrates how this range encompasses the literature candidates. The concentration is more obvious for the samples of Casewell et al. (2006) and Kraus & Hillenbrand (2007), which included proper motions in their membership

**Table 1**
Post-main-sequence Stars

| Name | R.A. (2000) (deg) | Decl. (2000) (deg) | $J$ (mag) | $eJ$ (mag) | $H$ (mag) | $eH$ (mag) | $K$ (mag) | $eK$ (mag) | $\mu_\alpha \cos \delta$ (mas yr$^{-1}$) | $\mu\delta$ (mas yr$^{-1}$) | $\Delta\mu$ (mas yr$^{-1}$) | SpTy | $B$ (mag) | $V$ (mag) | Comments |
|---|---|---|---|---|---|---|---|---|---|---|---|---|---|---|---|
| 12 Com | 185.62626 | +25.84614 | 3.781 | 0.254 | 3.401 | 0.216 | 3.236 | 0.244 | −10.9 | −9.6 | 0.5 | F6 III+A3V | 5.30 | 4.81 | ⋯ |
| 14 Com | 186.60021 | +27.26820 | 4.409 | 0.240 | 4.235 | 0.194 | 4.149 | 0.036 | −16.0 | −13.4 | 0.4 | F0p | 5.22 | 4.95 | ⋯ |
| 16 Com | 186.74703 | +26.82568 | 4.796 | 0.192 | 4.727 | 0.020 | 4.649 | 0.024 | −11.5 | −9.2 | 0.4 | A4 V | 5.05 | 4.96 | ⋯ |
| 31 Com | 192.92465 | +27.54068 | 3.629 | 0.292 | 3.367 | 0.218 | 3.260 | 0.286 | −11.0 | −8.3 | 0.3 | G0 IIIp | 4.39 | 4.94 | Outside 5 degs |
| 18 Com | 187.36261 | +24.10894 | 4.864 | 0.194 | 4.572 | 0.036 | 4.574 | 0.288 | −17.6 | 0.7 | 0.2 | F5 IV | 5.90 | 5.47 | not a member |

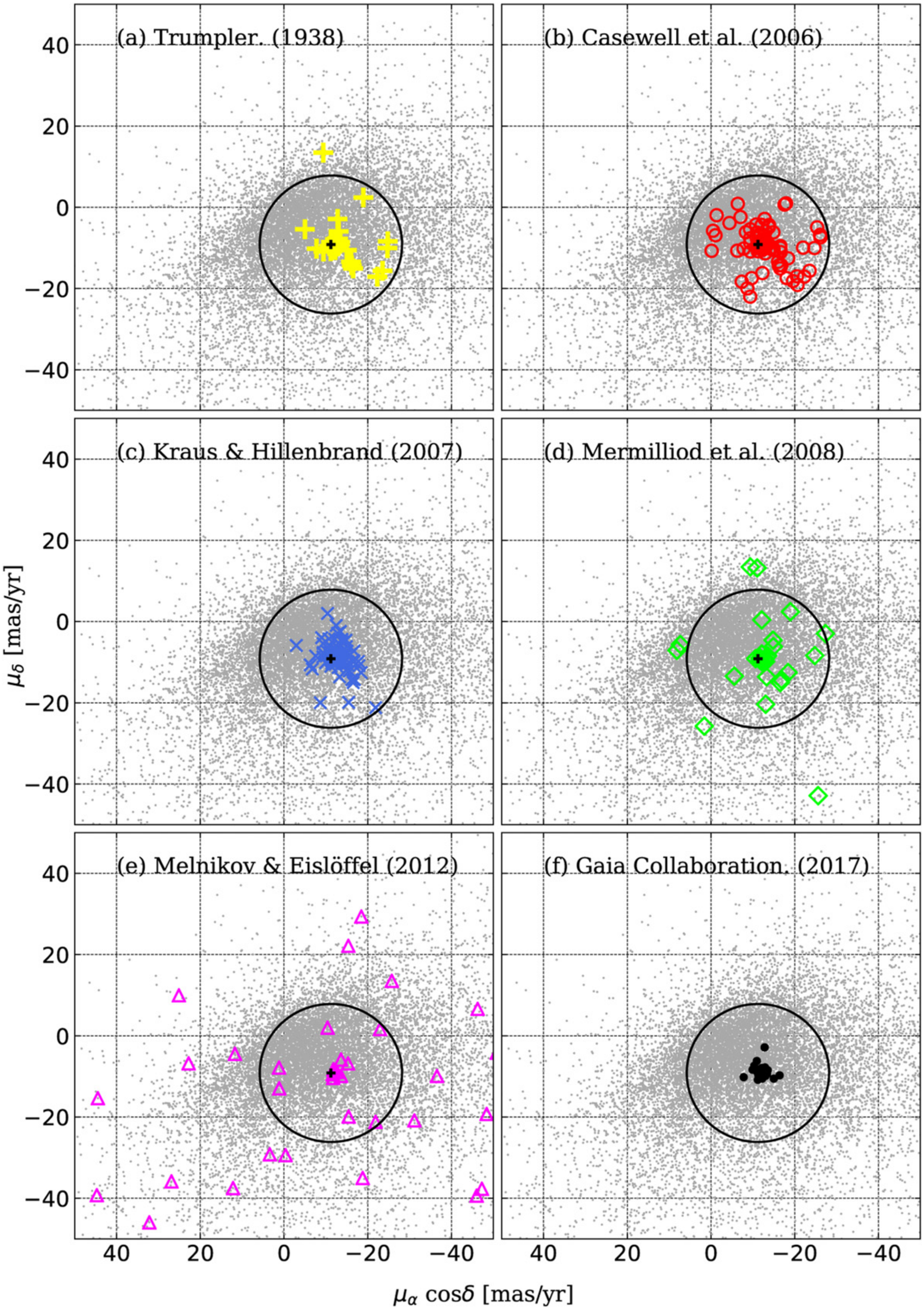


**Figure 4.** *Gaia*/DR2 proper motion vector plots for candidates identified by (a) Trumpler (1938), (b) Casewell et al. (2006), (c) Kraus & Hillenbrand (2007), (d) Mermilliod et al. (2008), (e) Melnikov & Eislöffel (2012), and (f) Gaia Collaboration et al. (2017). In each case, the black circle marks a radius of 17 mas yr$^{-1}$ centered at ($\mu_\alpha$ cos $\delta$, $\mu_\delta$) = (−11.21, −9.16) mas yr$^{-1}$, which indicates our selection range for bright candidates. For display clarity, only one in five field stars, selected randomly, is shown.

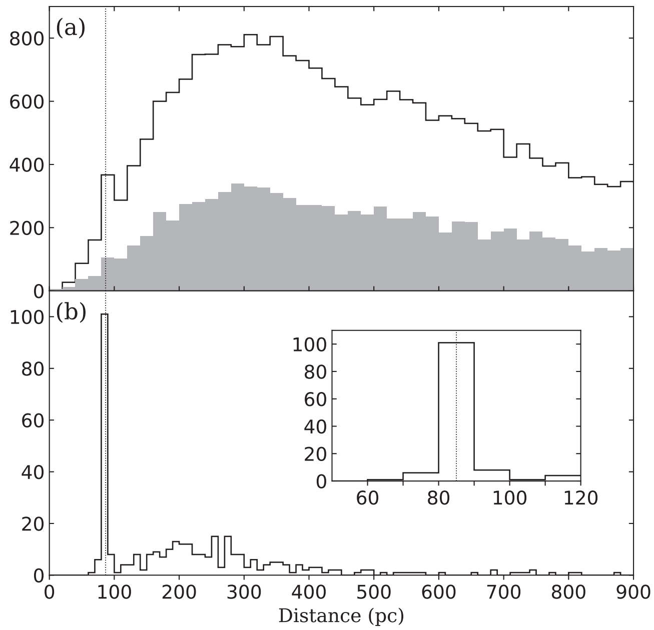


**Figure 5.** *Gaia*/DR2 parallax measurements of (a) all the stars toward the cluster region, and all the stars toward the field, which has a sky area of 9/25 or about one-third of the cluster region, and (b) our 393 preliminary candidates that passed the proper motion and isochrone selection. The inset expands to show the distance range 50–120 pc, in which most cluster members are distributed.

criteria, than for those of Mermilliod et al. (2008) or Melnikov & Eislöffel (2012), which applied no proper motion criteria.

Furthermore, a bright candidate is selected as being brighter than $J = 14$ mag with photometric errors $<0.15$ mag, and along the PARSEC isochrone (Bressan et al. 2012; Chen et al. 2014, 2015; Tang et al. 2014) bracketed with a color range $(-0.07, +0.3)$ in the $J$ versus $J - K_s$ color–magnitude diagram (CMD), $(-0.25, +0.15)$ in $J$ versus $J - H$, and $(-0.07, +0.11)$ in $H$ versus $H - K_s$. With these criteria, binary systems would still be selected. After excluding 23 candidates, all fainter than about $J \sim 12$ mag, considered as galaxies by SDSS (class = 3), a total of 450 sources satisfy the initial proper motion and CMD scrutiny. Of these, 393 have *Gaia*/DR2 counterparts.

Figure 5 plots the distance distributions of (a) all *Gaia* stars in the cluster region (within 5° radius), and all *Gaia* stars in the control field (3° radius), with a sky area 9/25 of the cluster region, and (b) the 393 preliminary candidates with *Gaia* measurements available. The clustering around 85 pc stands out clearly, particularly in (b). The fact that in (b) away from the peak the number does not increase much with distance, hence the space volume, in contrast to the case in (a), indicates an effective winnowing by proper motions and CMD.

Gaia Collaboration et al. (2017) analyzed a radius 10°.4 around Coma Ber, and reported 50 members based on *Gaia*/DR1 data. All their members have been confirmed by our selection (40 within and 9 outside the 5° cluster-centric radius), except BD+27 2139, which should have been in their list but is not, perhaps because of an editing glitch (Gaia Collaboration et al. 2017, their Table D.2 containing only 49 entries, though there should have been 50).

To bootstrap the three proper motion data sets used in this study, we compare the *Gaia*/DR2, URAT1, and UKIDSS/GCS measurements in the cluster region, shown in Figure 6. The *Gaia*/DR2 and URAT1 measurements are consistent with each other, and are used to supplement each other for bright candidates. There is, however, a systematic offset of UKIDSS/GCS measurements relative to those of URAT1, computed for all stars with $J = 12$–$15$ mag, i.e., common in both data sets, $(\Delta\mu_\alpha \cos\delta, \Delta\mu_\delta) = (-3.57, -0.61)$. After the offset is applied, the UKIDSS/GCS proper motion vector center $(-7.64, -8.55)$ mas yr$^{-1}$ is used to select faint members.

Distance is a critical parameter in membership identification. Although the apparent magnitude of a star in isochrone fitting and the proper motion both implicitly incorporate the distance criterion, ambiguity exists. In addition to direct parallax measurements, we have developed a distance estimator using the photometry data taken from the PS1, SDSS, and *YJHK* from UKIDSS, plus *W*1 and *W*2 from *WISE*. Our algorithm first estimates the spectral type of a star. This part is adapted from the *photo-type* method developed by Skrzypek et al. (2015), in which a combination of photometric colors of a target is compared against a database of templates of different spectral types, from which a match is chosen, in a least-squares sense, as the most probable spectral type. The work by Skrzypek et al. (2015) was devised for late-M, L, and T type dwarfs only, and we expand the templates to include earlier spectral types (see the Appendix). Once the spectral type is determined, the distance is then derived by comparison of the apparent magnitude and absolute magnitude in each band, rendering a median distance when all bands are considered. Our experiments using different stellar data sets with spectral types known to be K or M types indicate an accuracy within 1–2 subtypes in most cases, with the majority of interlopers being extragalactic or post-main-sequence objects, both expectedly rare in our field. Earlier than K type, the estimator still works reasonably fine, albeit with larger scattering; see Figure 7. Currently, no interstellar reddening is taken into account, and the algorithm is validated only for main-sequence stars. This distance estimator, which we call *phot-d*, offers an effective filtering by distance of stars that would have contaminated our member sample by chance inclusion in proper motion and CMD selection. More details on *phot-d* are given in the Appendix.

Figure 8 illustrates the $J$ versus $J - K_s$ CMD toward Coma Ber. Member candidates chosen on the basis of proper motions, distances, and isochrone are marked, together with those satisfying proper motion and isochrone conditions but having inconsistent distances, which would have been disguised as contaminants if no distance information were available. Also shown is the false-positive sample of the control field processed following the same selection procedure used for the cluster region. In this analysis, the distance range has been taken as 50–120 pc to account for the possible uncertainty of the *phot-d* distance. It is encouraging that the false-positive rate is low, particularly for the bright candidates ($\gtrsim 1\,M_\odot$) Within this distance range, there are 131 bright *Gaia* members, averaging 87.0 pc with a standard deviation (dispersion) 8.1 pc.

### 3.3. Faint Members

For faint stars, we have adopted the proper motion vector center $(\mu_\alpha \cos\delta, \mu_\delta) = (-7.64, -8.55)$ mas yr$^{-1}$ for UKIDSS/GCS, also within a radius of 17 mas yr$^{-1}$ for membership selection. In addition, a candidate is selected to be fainter than $J = 12$ mag, with photometric errors $<0.15$ mag, and along the DUSTY isochrone bracketed with a color range $(-0.35, +1.2)$ in the $Z$ versus $Z - K$ CMD, and

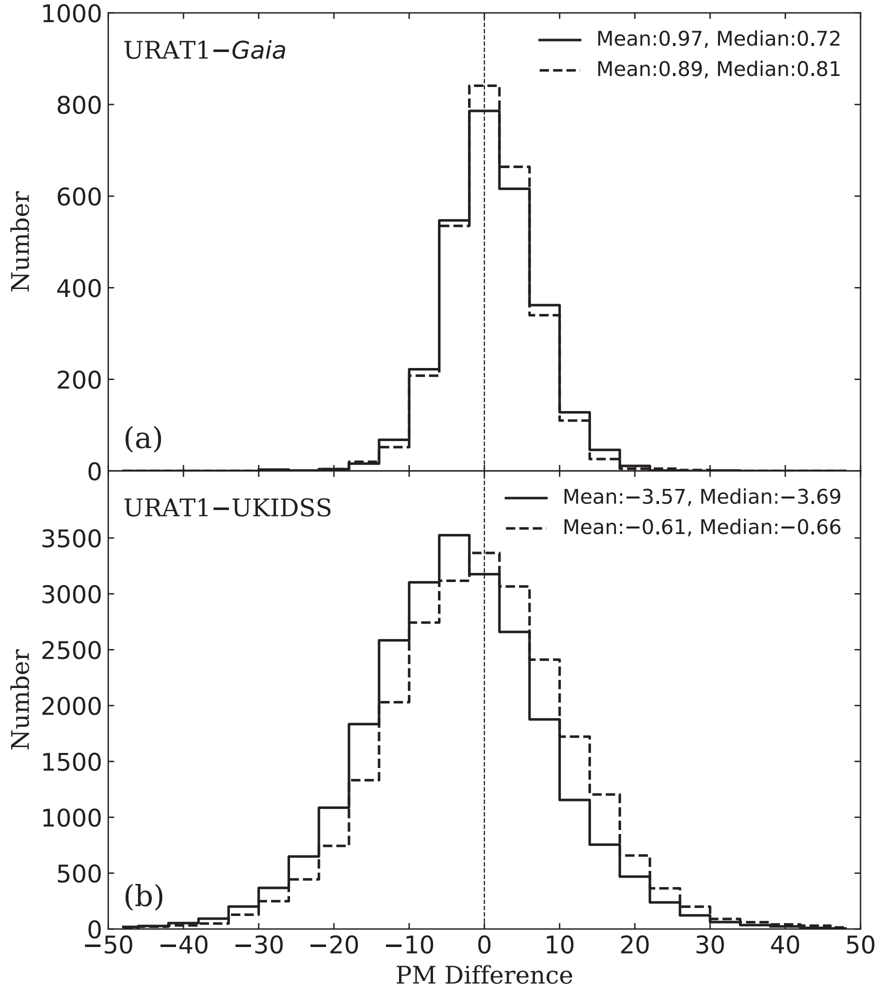


**Figure 6.** (a) Comparison of URAT1 and *Gaia*/DR2 proper motion values, in R.A. (solid line) and in decl. (dashed line). (b) Same as in (a), but for URAT1 and UKIDSS/GCS.

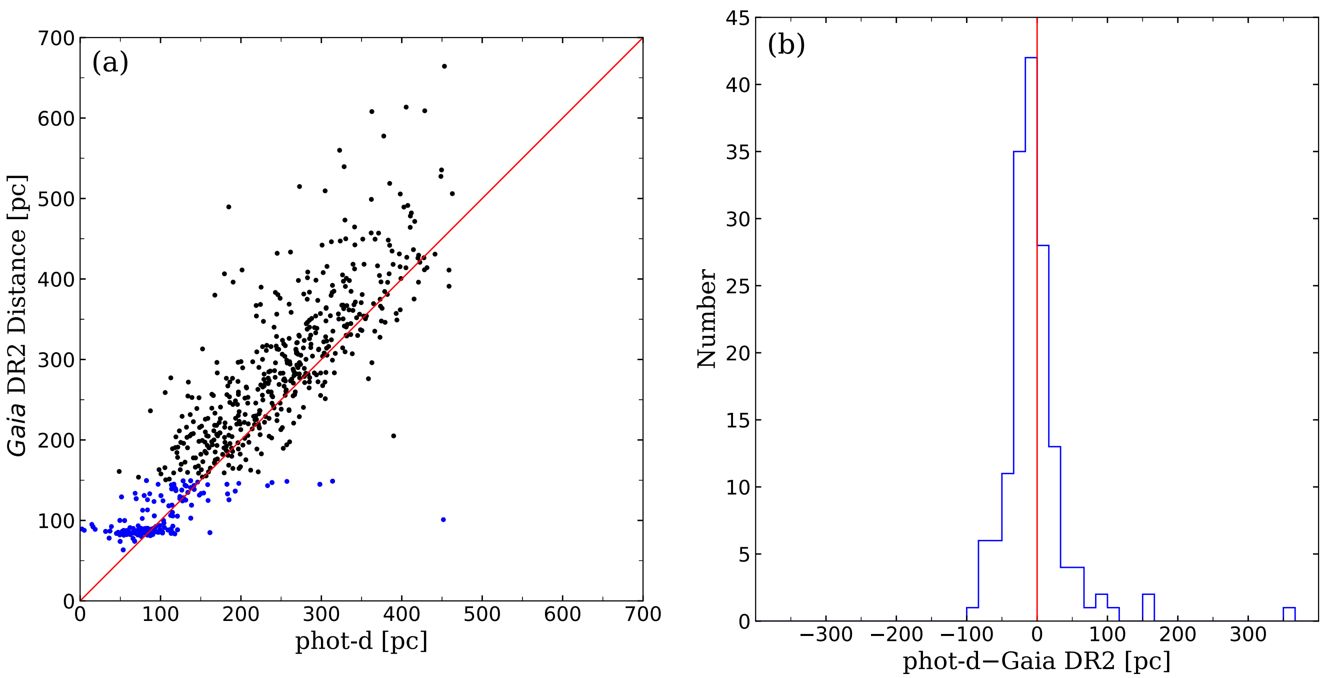


**Figure 7.** (a) *phot-d* determined distance vs. *Gaia* measured distance for a sample of preliminary candidates toward Coma Ber satisfying proper motions and CMD criteria. The red line with a unity slope shows equality. The black filled circles mark the relatively bright stars $J \sim 12$–14 mag, and the blue symbols represent the nearby stars with *Gaia* distances closer than 150 pc. (b) The difference between *phot-d* and *Gaia* distances for the nearby sample in (a).

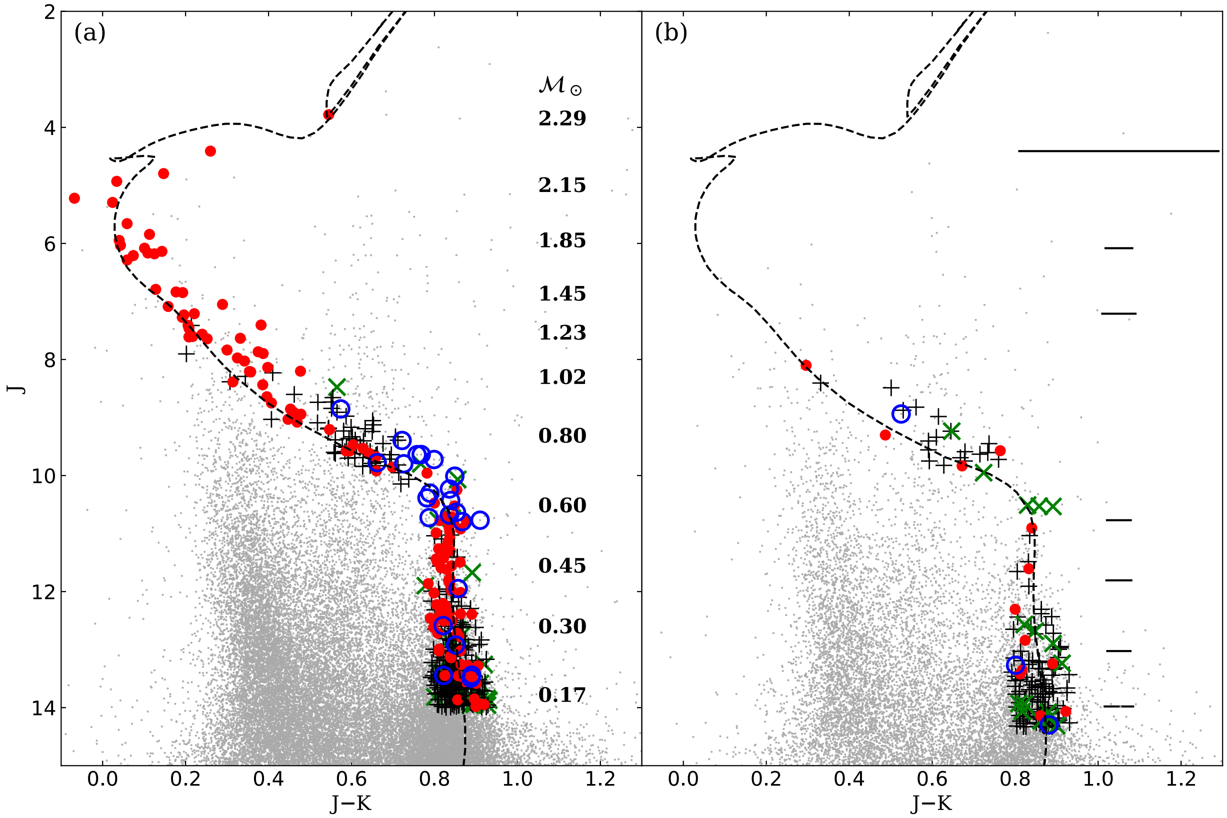


**Figure 8.** (a) 2MASS $J$ vs. $J-Ks$ for the bright sample in the cluster region. The gray dots represent all 2MASS sources. The circles mark the candidates satisfying the proper motion and isochrone criteria, and are further constrained, respectively, by parallax distances (in red filled circles) and *phot-d* distances (in blue open circles). Those satisfying both proper motion and isochrone selection but otherwise rejected by distances, are represented by black pluses (with *Gaia* distances) or by green crosses (with *phot-d* distances. Stellar masses, per the PARSEC isochrones, are indicated. (b) The same as (a) but for the control sample, with the same symbols as in (a). The stars that satisfied all criteria of proper motions, isochrone, and distance here are false positives. Typical errors in 2MASS $J-K_s$ colors are presented as horizontal bars to the right.

(−0.1, +0.5) in $J$ versus $J-K$, as shown in Figure 9. The ranges of colors are chosen to be deliberately wide to allow for uncertainties in photometry/color and also in isochrones. The distance range, as chosen for the bright sample, is chosen to be 50–120 pc for either the *Gaia* or the *phot-d* distances.

Note that in $J$ versus $J-K$, which is often used to identify substellar objects, the isochrone passes through populated regions, so such a CMD is not as discriminating as those involving shorter wavelengths such as $Z$ versus $Z-K$ for low-mass objects. Our investigation hence relies primarily on $Z$ versus $Z-K$, though for very cool objects a marked flux suppression sometimes renders detection at neither $Y$ nor $Z$ in UKIDSS/GCS. For these, analysis with $J$ versus $J-K$ would be applied. The lesson is that there are no preferred colors to identify cool objects, and a combination of CMDs must be iterated. As a comparison, Figure 10 presents how literature candidates behave in our diagnostic 2MASS $J$ versus $J-K_s$ and UKIDSS/GCS $Z$ versus $Z-K$ CMDs, overlaid with several theoretical 800 Myr isochrones adopting the average distance 85 pc. We note that for a nearby cluster such as Coma Ber, assuming a single distance in a CMD would introduce intrinsic scattering unless absolute magnitudes are plotted (see for example Figure 3). While the bright literature candidates by and large follow the model isochrones, the faint ones are discrepant.

Combining the bright (Section 3.2) and faint (Section 3.3) candidates together results in 194 candidates within the cluster region. This sample is spatially complete, notwithstanding the UKIDSS voids, and forms the basis of our characterization of the cluster. The candidates are listed in Table 2. The first column gives the running number. Columns 2 and 3 are the coordinates, followed by columns 4 to 9 representing $J$ mag, its error, $H$ mag, its error, and $K$ mag and its error. Columns 10 to 12 give the proper motions and the error. Column 13 lists the distance, followed by column 14, which contains the references if the star is a known literature candidate. The last column indicates the data source, where "1" stands for 2MASS photometry ($JHK_s$) plus *Gaia*/DR2 proper motions, "2" stands for 2MASS photometry ($JHK_s$) plus URAT-1 proper motions, "3" stands for UKIDSS/GCS ($JHK$) plus *Gaia*/DR2 proper motions, and "4" means that $JHK$ photometry and proper motion are both from UKIDSS/GCS, with no transformation between 2MASS and UKIDSS photometric measurements.

Candidates in Table 2 are categorized as (1) those with parallax distances (Nos. 1–154; this is the most reliable member list to our knowledge to date of the Coma Ber cluster); and (2) the other 38 with distances estimated by *phot-d* (Nos. 155–192). For sources with parallax measurements but $\varpi/\Delta\varpi < 10$, their *photo-d* distances are adopted. In each category the entries are in ascending R.A. order.

The criterion of the ratio $\varpi/\Delta\varpi > 10$ for *Gaia*/DR2 data is biased against a distant source for which $\varpi$ would be small (so is the ratio) even though $\Delta\varpi$ is already relatively small. These sources tend to be distributed in the vertical segment of the $J$

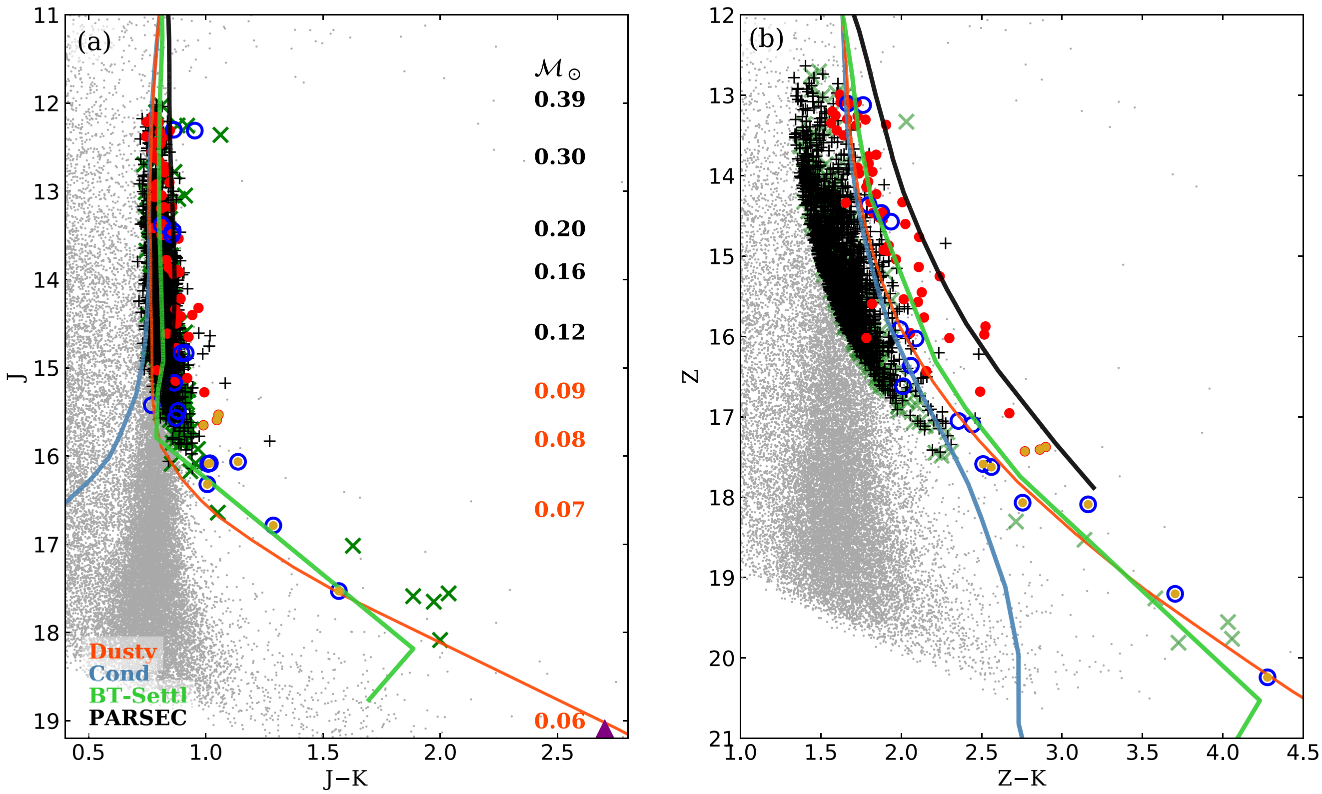


**Figure 9.** (a) The $J$ vs. $J-K$ CMD, just as in Figure 8, with the same symbols, but for the faint sample using UKIDSS/GCS data. The additional golden dots mark the brown dwarf candidates identified in this work. The stellar masses, per the PARSEC (the black line) or the DUSTY models (the orange line), are indicated. Additional isochrones, those of Cond (the blue line) and BT-Settl (the green line), are also shown. (b) The $Z$ vs. $Z-K$ CMD, using the same symbols as in (a). One source marked as a purple triangle in (a) does not appear here because of no detection at $Z$. For display clarity, only one in every five field stars (as gray dots), selected randomly, is shown.

versus $J-Ks$ CMD. They are hence likely background giants; as such, *phot-d*, which is valid for dwarfs only, would underestimate the distances. At the moment we do not have an effective method to remove these individual contaminants from the member list, except by statistical subtraction by the control sample.

There are individual objects considered as member candidates in the literature but outside the 5° radius. A total of 15 have been reaffirmed by our analysis, including, for example, 31 Com, presented above as a post-main-sequence member (Section 3.1), and two reported by Kraus & Hillenbrand (2007): HD 111878 with a *Gaia* distance 85.1 pc, and HD 109390 at 120.1 pc (close to the limit of our distance range). This selected sample is spatially incomplete and thus is not included in further analysis, but is listed in Table 3 for reference, with the same table format as in Table 2, except with no last column because all data are from 2MASS and *Gaia*/DR2.

For potential usefulness, we also summarize in Table 5 the literature candidates rejected by our selection. The table is in a two-column format arranged in ascending R.A. order. For each star, the coordinates, references for candidacy, and an offending code in our analysis are given: 1 = rejection by proper motions, 2 = rejection by CMD, 4 = rejection by distance. The code is additive, so, for example, a literature candidate that has consistent proper motions but is inconsistent with being a member in CMD position and in distance has a code = 6.

### 3.4. Brown Dwarf Members

Any member fainter than $Z = 17.3$ mag has a mass less than $0.08\,M_\odot$, and is therefore a brown dwarf. There are several lines of evidence to further substantiate its brown dwarf nature. First, late-M, L, and T dwarfs are known to have UKIDSS colors different from those of field stars (Hewett et al. 2006), and all our brown dwarf candidates indeed have colors, shown in Figure 11, consistent with being M- or L-type objects. Second, all these candidates have spectral types estimated by *phot-d* as being brown dwarfs.

Moreover, while very-low-mass objects have distinctly red $W1-W2$ colors (Kirkpatrick et al. 2011) owing to the lack of methane absorption at $W2$ (4.6 $\mu$m) relative to the flux at $W1$ (3.4 $\mu$m), their $W3$ (12 $\mu$m) and $W4$ (22 $\mu$m) fluxes often fall below the sensitivity limits of *WISE* unless they are located in the solar vicinity (see, for example, Scholz et al. 2011).

Among the efforts to identify brown dwarfs in Coma Ber, the spectroscopic study by Casewell et al. (2014) led to confirmation of an M9 (their cbd34, R.A. = 12:23:57.37, decl. = +24:53:29.0, J2000, $J = 15.94$ mag), an L1 (their cbd67, R.A. = 12:18:32.71, decl. = +27:37:31.3, J2000, $J = 17.68$ mag), and an L2 (their cbd40, R.A. = 12:16:59.89, decl. = +27:20:05.5, J2000, $J = 16.30$ mag), among which cbd40 was stripped of its membership on the basis of its brightness and colors. Our candidate list includes cbd34 but not cbd67, which satisfies neither the proper motion nor the photometric criterion, and is therefore a field brown dwarf. West et al. (2011) compiled a catalog of spectroscopic M dwarfs on the

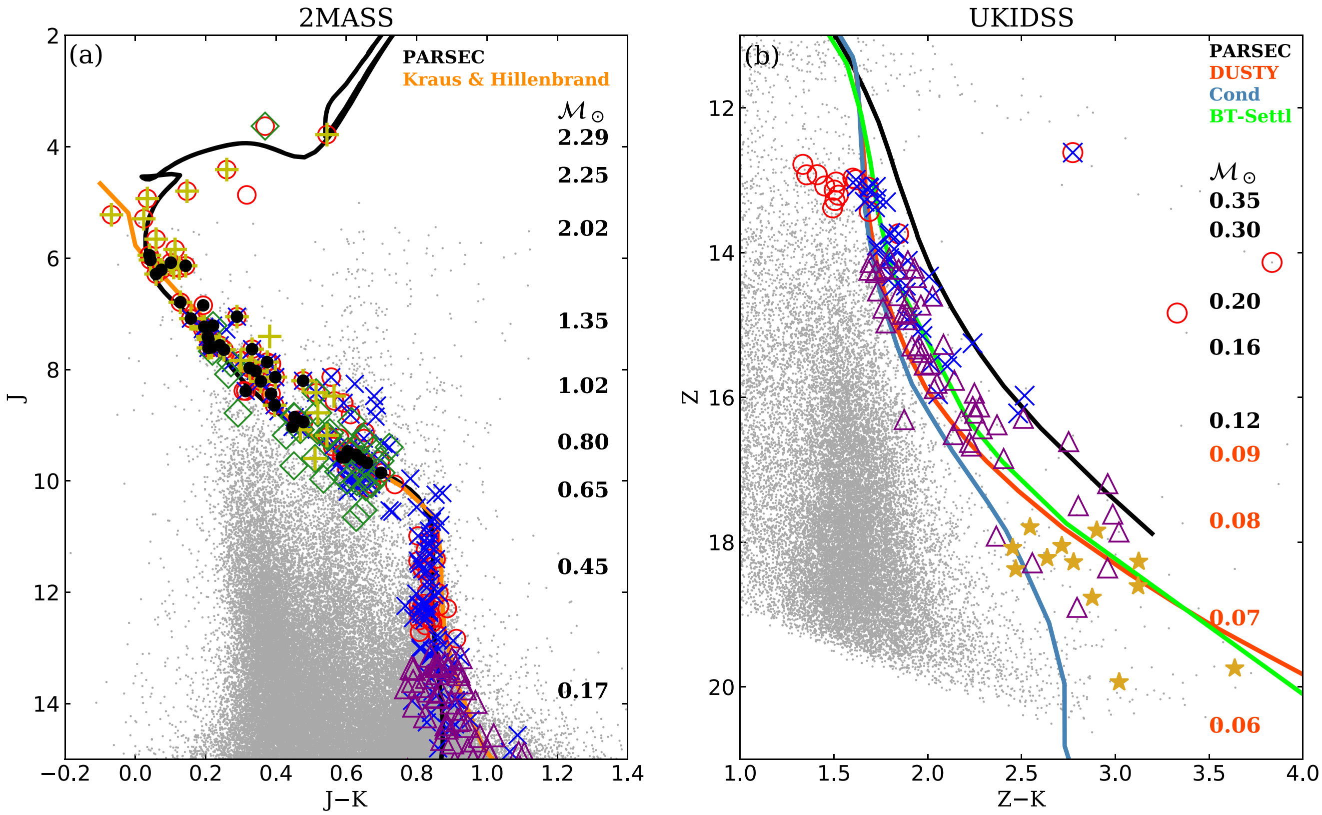


**Figure 10.** Color–magnitude diagrams for literature candidates in (a) 2MASS $J$ vs. $J - K_s$ and (b) UKIDSS/GCS $Z$ vs. $Z - K$. Data include those from (Trumpler 1938, in plus symbols), Casewell et al. (2006, open circles) Kraus & Hillenbrand (2007, in cross), Mermilliod et al. (2008, open diamonds), Melnikov & Eislöffel (2012, in open triangles), Gaia Collaboration et al. (2017, dots), and Casewell et al. (2005, their BD candidates, star symbols). Also plotted are lines depicting evolutionary models of PARSEC (in black), Dusty (in orange), Cond (in blue), BT-Settl (in green), and an empirical dwarf sequence from Kraus & Hillenbrand (2007, in orange). The stellar masses according to PARSEC or Dusty are labeled. For display clarity, only one in every five UKIDSS field stars (as gray dots), selected randomly, is shown.

basis of the Sloan Digital Sky Survey DR7. Among the M dwarfs in our cluster region, 10 satisfy our selection criteria of proper motions, CMD, and distance, and indeed have been included in our list.

Table 4 summarizes the properties of the substellar objects, a subset of the member candidates in Table 2. Following the same identification numbers as in Table 2 in the first column, the next columns list, respectively, the coordinates, UKIDSS $Z$, $Y$, $J$, $H$, and $K1$ magnitudes, and then the UKIDSS proper motions. The last two columns compare the spectral type determined with spectroscopy, as reported in the literature or observed by us, and the spectral type estimated with *phot-d*. In general, the spectral typing with *phot-d* is in agreement within 1–2 subtypes with observations. This gives us confidence in our *phot-d* method. The first six sources in Table 4 are all of late-M types known in the literature (West et al. 2011; Casewell et al. 2014), and we have confirmed their membership. The M9 objects, namely Nos. 176, 55, and 130, were the coolest known members in Coma Ber before our work.

In Table 4 there are a few miscellaneous objects , A, B, and C, that are not classified as member candidates but are worth clarification. Stars A and B have similar infrared colors (from $Z$ to *WISE* $W2$) as those of known brown dwarfs, as seen in the two-color diagrams shown in Figure 11. Yet, at shorter wavelengths object A has PS1 measurements $g_{P1} = 19.97$ mag, $r_{P1} = 18.73$ mag, and $i_{P1} = 17.61$ mag, and object B has $g_{P1} = 20.55$ mag, $r_{P1} = 19.30$ mag, and $i_{P1} = 18.03$ mag. Compared with the mean values and standard deviation of the M-type brown dwarfs in Table 4, $g_{P1} = 21.51 \pm 0.56$ mag, $r_{P1} = 21.94 \pm 0.19$ mag, and $i_{P1} = 19.54 \pm 0.32$ mag, the two stars stand out as significantly brighter. The *phot-d* analysis suggests both to be of early-M types. While the binarity of a hot plus a cold component may explain the brightness inconsistency, we do not have evidence at the moment as to the nature of either star.

Object C has *JHK* magnitudes and proper motions consistent with being substellar, but has $Z$ and $Y$ magnitudes below the UKIDSS/GCS limits. It is the only source in the table that has been clearly detected not only in $W1$ and $W2$, but also in $W3$ and $W4$ (see Figure 12.) It is likely a galaxy.

### *3.4.1. Follow-up Spectroscopy*

Confirmation spectra of the brown dwarf candidates were acquired with Palomar/TripleSpec or with Gemini/GNIRS. Three targets, No. 159, A, and B, were observed using TripleSpec (Herter et al. 2008) on 2016 December 14, with a slit width 1″. The sky was clear and the observations were executed at an airmass of about 1.20. The standard A-B-B-A nodding sequence was followed along the slit to record target and sky spectra. The exposure time per pointing was 300 s, with a total integration of 1200 s for each target. Flat-fields and argon lamp spectra were taken after every set of target observations. A nearby A0 V star was observed for each target for telluric correction, as well as for flux calibration.

SPEXTOOL package version 4.1 (Vacca et al. 2003; Cushing et al. 2004) has been used for processing of the

**Table 2**
Candidate Members of Coma Ber

| No. (1) | R.A. (2000) (deg) (2) | Decl. (2000) (deg) (3) | $J$ (mag) (4) | Jerr (mag) (5) | $H$ (mag) (6) | Herr (mag) (7) | $Ks$ (mag) (8) | Kserr (mag) (9) | $\mu_\alpha \cos\delta$ mas yr$^{-1}$ (10) | $\mu_\delta$ mas yr$^{-1}$ (11) | $\Delta\mu$ mas yr$^{-1}$ (12) | Dist (pc) (13) | Ref.[a] (14) | Data[b] (15) |
|---|---|---|---|---|---|---|---|---|---|---|---|---|---|---|
| Distance by Parallax | | | | | | | | | | | | | | |
| 1 | 181.09398 | 24.02144 | 12.787 | 0.002 | 12.297 | 0.001 | 11.962 | 0.001 | −12.3 | −9.4 | 0.2 | 85.4 | c | 3 |
| 2 | 181.09694 | 24.82066 | 8.750 | 0.023 | 8.414 | 0.018 | 8.343 | 0.019 | −12.5 | −9.9 | 0.1 | 82.4 | cf | 1 |
| 3 | 181.36050 | 26.33820 | 10.524 | 0.031 | 9.871 | 0.031 | 9.676 | 0.035 | −3.8 | −17.8 | 0.1 | 74.1 | | 1 |
| 4 | 181.36131 | 26.33937 | 10.783 | 0.022 | 10.152 | 0.018 | 9.937 | 0.019 | −4.9 | −20.6 | 0.1 | 73.9 | | 1 |
| 5 | 181.38475 | 22.90031 | 13.488 | 0.002 | 12.966 | 0.002 | 12.656 | 0.002 | −7.8 | −12.5 | 0.2 | 92.8 | | 3 |
| 6 | 181.39774 | 25.02538 | 15.531 | 0.007 | 14.980 | 0.007 | 14.477 | 0.008 | −12.9 | −9.7 | 1.1 | 87.7 | | 3 |
| 7 | 181.53316 | 24.35440 | 12.719 | 0.022 | 12.118 | 0.021 | 11.864 | 0.020 | −11.3 | −17.4 | 0.2 | 119.0 | | 1 |
| 8 | 181.63802 | 23.86454 | 13.482 | 0.027 | 12.958 | 0.032 | 12.592 | 0.025 | −12.4 | −9.6 | 0.2 | 84.4 | c | 1 |
| 9 | 181.79992 | 26.06119 | 13.116 | 0.024 | 12.572 | 0.023 | 12.278 | 0.022 | −12.2 | −9.2 | 0.2 | 84.3 | c | 1 |
| 10 | 181.92396 | 24.21646 | 9.959 | 0.022 | 9.332 | 0.022 | 9.177 | 0.017 | −9.3 | −8.7 | 0.1 | 93.4 | c | 1 |
| 11 | 181.99044 | 25.58648 | 9.534 | 0.022 | 9.028 | 0.019 | 8.906 | 0.017 | −9.9 | −8.3 | 0.2 | 92.7 | cf | 1 |
| 12 | 182.03835 | 24.72508 | 13.279 | 0.024 | 12.711 | 0.023 | 12.374 | 0.023 | −11.7 | −8.0 | 0.3 | 85.2 | c | 1 |
| 13 | 182.37284 | 29.32707 | 10.790 | 0.019 | 10.126 | 0.021 | 9.913 | 0.017 | −17.4 | −15.4 | 0.3 | 94.8 | | 1 |
| 14 | 182.67053 | 26.42563 | 14.321 | 0.004 | 13.802 | 0.003 | 13.352 | 0.003 | −11.3 | −8.3 | 0.6 | 82.0 | | 3 |
| 15 | 182.69202 | 27.28147 | 5.659 | 0.029 | 5.668 | 0.031 | 5.600 | 0.033 | −12.4 | −9.5 | 0.2 | 86.9 | ab | 1 |
| 16 | 182.78072 | 25.99015 | 8.387 | 0.023 | 8.115 | 0.017 | 8.073 | 0.033 | −11.9 | −9.3 | 0.1 | 86.8 | bcf | 1 |
| 17 | 182.89646 | 29.37899 | 9.575 | 0.022 | 9.053 | 0.027 | 8.979 | 0.024 | −11.8 | −8.8 | 0.1 | 89.3 | cf | 1 |
| 18 | 182.94819 | 24.87139 | 13.938 | 0.003 | … | … | 13.075 | 0.003 | −12.3 | −10.3 | 0.2 | 83.8 | c | 3 |
| 19 | 183.10368 | 27.38006 | 7.274 | 0.024 | 7.130 | 0.021 | 7.082 | 0.021 | −12.2 | −9.4 | 0.1 | 85.7 | abc | 1 |
| 20 | 183.17821 | 25.22843 | 13.406 | 0.022 | 12.835 | 0.026 | 12.518 | 0.025 | −11.8 | −7.9 | 0.2 | 88.4 | c | 1 |
| 21 | 183.22177 | 26.25037 | 9.577 | 0.018 | 9.106 | 0.016 | 8.990 | 0.018 | −12.1 | −9.5 | 0.1 | 86.3 | bcf | 1 |
| 22 | 183.33962 | 23.37229 | 12.619 | 0.023 | 12.053 | 0.023 | 11.821 | 0.022 | 4.3 | −10.3 | 0.1 | 99.0 | | 1 |
| 23 | 183.43287 | 22.88796 | 7.211 | 0.027 | 7.052 | 0.017 | 6.990 | 0.033 | −13.5 | −8.4 | 0.2 | 86.6 | cdf | 1 |
| 24 | 183.44299 | 30.34077 | 13.582 | 0.027 | 13.012 | 0.033 | 12.681 | 0.026 | −11.2 | −19.3 | 0.7 | 99.8 | | 1 |
| 25 | 183.61048 | 23.23399 | 11.806 | 0.024 | 11.244 | 0.031 | 10.972 | 0.022 | −11.3 | −8.9 | 0.1 | 91.0 | | 1 |
| 26 | 183.81815 | 29.35072 | 12.506 | 0.021 | 11.952 | 0.021 | 11.684 | 0.018 | −11.8 | −9.3 | 0.1 | 87.4 | c | 1 |
| 27 | 183.88110 | 25.06697 | 13.022 | 0.021 | 12.423 | 0.020 | 12.159 | 0.023 | −12.1 | −9.1 | 0.2 | 88.4 | c | 1 |
| 28 | 184.00348 | 28.09662 | 11.077 | 0.024 | 10.525 | 0.033 | 10.240 | 0.018 | −10.9 | −7.7 | 0.6 | 86.8 | bc | 1 |
| 29 | 184.03485 | 25.76034 | 7.232 | 0.026 | 7.117 | 0.047 | 7.036 | 0.017 | −12.2 | −10.5 | 0.1 | 85.3 | abcf | 1 |
| 30 | 184.09773 | 28.41948 | 13.866 | 0.026 | 13.263 | 0.027 | 13.010 | 0.027 | −10.4 | 2.0 | 0.3 | 85.2 | ce | 1 |
| 31 | 184.15536 | 26.89944 | 12.225 | 0.022 | 11.680 | 0.024 | 11.420 | 0.018 | −12.3 | −9.4 | 0.1 | 86.8 | bc | 1 |
| 32 | 184.17173 | 26.77747 | 13.141 | 0.020 | 12.563 | 0.024 | 12.301 | 0.023 | −11.7 | −10.4 | 0.2 | 85.9 | ce | 1 |
| 33 | 184.33914 | 25.48123 | 13.274 | 0.023 | 12.671 | 0.023 | 12.394 | 0.021 | −11.9 | −8.3 | 0.2 | 87.3 | ce | 1 |
| 34 | 184.42752 | 30.98329 | 12.900 | 0.002 | 12.389 | 0.001 | 12.054 | 0.001 | −21.8 | −13.6 | 0.1 | 81.1 | | 3 |
| 35 | 184.46208 | 25.57132 | 7.086 | 0.018 | 6.982 | 0.024 | 6.928 | 0.017 | −11.3 | −9.6 | 0.1 | 89.4 | abcf | 1 |
| 36 | 184.55316 | 26.82093 | 12.016 | 0.022 | 11.459 | 0.021 | 11.153 | 0.020 | −11.0 | −6.3 | 0.7 | 78.0 | bc | 1 |
| 37 | 184.59100 | 25.40361 | 14.498 | 0.004 | … | … | 13.623 | 0.004 | −13.6 | −9.9 | 0.4 | 82.4 | e | 3 |
| 38 | 184.59132 | 27.74508 | 12.992 | 0.024 | 12.392 | 0.030 | 12.181 | 0.018 | −12.2 | −9.8 | 0.2 | 83.9 | c | 1 |
| 39 | 184.65070 | 23.12004 | 7.635 | 0.019 | 7.386 | 0.023 | 7.303 | 0.020 | −15.0 | −10.5 | 0.6 | 85.7 | abcf | 1 |
| 40 | 184.75610 | 24.84615 | 7.837 | 0.056 | 7.555 | 0.036 | 7.537 | 0.018 | −16.2 | −14.3 | 0.2 | 85.0 | abc | 1 |
| 41 | 184.75839 | 26.00832 | 6.082 | 0.026 | 6.004 | 0.049 | 5.981 | 0.023 | −12.5 | −8.5 | 0.3 | 86.4 | abf | 1 |
| 42 | 184.81311 | 28.28071 | 12.385 | 0.029 | 11.769 | 0.030 | 11.522 | 0.022 | −3.0 | −15.6 | 0.1 | 110.6 | | 1 |
| 43 | 184.82992 | 23.03464 | 5.948 | 0.021 | 5.969 | 0.021 | 5.908 | 0.020 | −12.6 | −9.6 | 0.1 | 85.4 | abf | 1 |
| 44 | 184.86810 | 24.28422 | 7.867 | 0.019 | 7.557 | 0.044 | 7.492 | 0.027 | −12.8 | −2.9 | 0.3 | 83.8 | abcf | 1 |
| 45 | 184.90816 | 26.57905 | 12.776 | 0.029 | 12.239 | 0.033 | 11.917 | 0.023 | −16.6 | −9.6 | 0.7 | 87.9 | bc | 1 |
| 46 | 184.96089 | 28.46432 | 6.209 | 0.019 | 6.192 | 0.034 | 6.135 | 0.024 | −12.3 | −9.0 | 0.1 | 85.6 | abf | 1 |
| 47 | 184.96843 | 31.16615 | 15.278 | 0.006 | 14.718 | 0.006 | 14.284 | 0.006 | −11.9 | −10.6 | 0.8 | 80.0 | | 3 |
| 48 | 185.06034 | 25.43537 | 12.214 | 0.001 | … | … | 11.464 | 0.001 | −11.8 | −8.7 | 0.1 | 92.4 | c | 3 |
| 49 | 185.16139 | 29.65041 | 12.392 | 0.024 | 11.790 | 0.028 | 11.502 | 0.025 | −7.7 | −23.4 | 0.2 | 65.4 | | 1 |
| 50 | 185.16438 | 29.64768 | 11.495 | 0.022 | 10.871 | 0.028 | 10.633 | 0.025 | −7.8 | −23.9 | 0.1 | 65.6 | | 1 |
| 51 | 185.18983 | 25.76584 | 7.974 | 0.021 | 7.740 | 0.033 | 7.649 | 0.026 | −12.2 | −8.3 | 0.1 | 84.4 | abcf | 1 |
| 52 | 185.31501 | 26.15388 | 9.614 | 0.019 | 9.087 | 0.024 | 8.972 | 0.020 | −11.8 | −9.4 | 0.1 | 84.9 | bcdf | 1 |
| 53 | 185.36137 | 24.99700 | 6.792 | 0.020 | 6.742 | 0.026 | 6.664 | 0.017 | −12.0 | −9.5 | 0.1 | 87.7 | abf | 1 |
| 54 | 185.41950 | 27.13081 | 10.712 | 0.023 | 10.125 | 0.025 | 9.887 | 0.019 | −11.8 | −8.9 | 0.1 | 87.3 | | 1 |
| 55 | 185.42258 | 21.68386 | 15.651 | 0.008 | 15.119 | 0.009 | 14.661 | 0.011 | −10.6 | −8.2 | 1.3 | 102.4 | | 3 |
| 56 | 185.45422 | 26.54907 | 8.214 | 0.026 | 7.863 | 0.027 | 7.857 | 0.027 | −12.5 | −8.1 | 0.1 | 86.5 | abcf | 1 |
| 57 | 185.48395 | 27.30948 | 7.565 | 0.024 | 7.399 | 0.042 | 7.325 | 0.020 | −13.4 | −9.0 | 0.1 | 85.3 | abcf | 1 |
| 58 | 185.55134 | 30.85934 | 13.940 | 0.028 | 13.344 | 0.026 | 13.030 | 0.028 | −22.5 | −14.0 | 0.3 | 77.5 | | 1 |
| 59 | 185.56031 | 25.44897 | 13.980 | 0.028 | 13.397 | 0.032 | 13.080 | 0.024 | −11.6 | −9.5 | 0.3 | 87.3 | ce | 1 |
| 60 | 185.60311 | 22.46410 | 7.604 | 0.019 | 7.394 | 0.018 | 7.387 | 0.020 | −11.8 | −9.9 | 0.1 | 85.7 | abcf | 1 |
| 61 | 185.62626 | 25.84614 | 3.781 | 0.254 | 3.401 | 0.216 | 3.236 | 0.244 | −10.8 | −9.5 | 0.5 | 84.5 | ab | 1 |

**Table 2**
(Continued)

| No. (1) | R.A. (2000) (deg) (2) | Decl. (2000) (deg) (3) | $J$ (mag) (4) | Jerr (mag) (5) | $H$ (mag) (6) | Herr (mag) (7) | $Ks$ (mag) (8) | Kserr (mag) (9) | $\mu_\alpha \cos\delta$ mas yr$^{-1}$ (10) | $\mu_\delta$ mas yr$^{-1}$ (11) | $\Delta\mu$ mas yr$^{-1}$ (12) | Dist (pc) (13) | Ref.[a] (14) | Data[b] (15) |
|---|---|---|---|---|---|---|---|---|---|---|---|---|---|---|
| 62 | 185.63074 | 25.82848 | 7.406 | 0.029 | 7.150 | 0.026 | 7.024 | 0.018 | −5.0 | −5.4 | 1.2 | 66.2 | a | 1 |
| 63 | 185.66225 | 27.77868 | 14.418 | 0.004 | 13.904 | 0.003 | 13.524 | 0.004 | −11.8 | −8.3 | 0.4 | 90.2 | ce | 3 |
| 64 | 185.75796 | 21.56379 | 12.469 | 0.024 | 11.874 | 0.023 | 11.661 | 0.020 | −23.2 | −0.9 | 0.1 | 118.1 | | 1 |
| 65 | 185.76285 | 22.13122 | 11.863 | 0.022 | 11.294 | 0.022 | 11.078 | 0.020 | −1.4 | −22.6 | 0.1 | 79.8 | | 1 |
| 66 | 185.78496 | 25.85135 | 8.027 | 0.020 | 7.762 | 0.021 | 7.685 | 0.023 | −12.3 | −8.7 | 0.3 | 87.7 | abcf | 1 |
| 67 | 185.80006 | 23.93748 | 12.204 | 0.022 | 11.614 | 0.022 | 11.384 | 0.018 | −11.7 | −9.1 | 0.2 | 89.9 | bc | 1 |
| 68 | 185.80644 | 26.03844 | 12.025 | 0.020 | 11.519 | 0.016 | 11.226 | 0.019 | −14.9 | −12.0 | 0.5 | 81.7 | c | 1 |
| 69 | 185.86747 | 25.89440 | 9.920 | 0.022 | 9.354 | 0.022 | 9.260 | 0.020 | −12.0 | −9.8 | 0.1 | 86.2 | bcd | 1 |
| 70 | 185.92082 | 26.97991 | 7.461 | 0.021 | 7.334 | 0.080 | 7.253 | 0.021 | −12.2 | −7.9 | 0.1 | 87.5 | abcf | 1 |
| 71 | 185.92423 | 26.60147 | 8.137 | 0.023 | 7.791 | 0.033 | 7.739 | 0.020 | −13.0 | −9.5 | 0.2 | 92.4 | abcf | 1 |
| 72 | 185.94668 | 23.24565 | 9.677 | 0.021 | 9.129 | 0.022 | 9.018 | 0.018 | −12.6 | −10.0 | 0.1 | 85.1 | bf | 1 |
| 73 | 185.95401 | 24.13215 | 10.474 | 0.024 | 9.880 | 0.030 | 9.674 | 0.019 | −17.9 | −10.9 | 0.4 | 85.9 | c | 1 |
| 74 | 185.98129 | 23.41443 | 11.591 | 0.020 | 10.995 | 0.023 | 10.775 | 0.017 | −11.3 | −9.3 | 0.1 | 88.2 | bc | 1 |
| 75 | 186.01438 | 25.85121 | 6.179 | 0.024 | 6.075 | 0.047 | 6.054 | 0.018 | −13.0 | −5.9 | 0.5 | 95.0 | ab | 1 |
| 76 | 186.02385 | 26.12857 | 9.080 | 0.027 | 8.762 | 0.065 | 8.611 | 0.021 | −11.7 | −9.0 | 0.1 | 88.9 | acd | 1 |
| 77 | 186.04529 | 23.99336 | 12.266 | 0.021 | 11.664 | 0.020 | 11.452 | 0.018 | −12.8 | −9.0 | 0.1 | 82.4 | bc | 1 |
| 78 | 186.04673 | 26.88793 | 10.921 | 0.031 | 10.265 | 0.030 | 10.058 | 0.018 | −11.3 | −9.4 | 0.1 | 86.3 | | 1 |
| 79 | 186.07718 | 26.09857 | 4.930 | 0.037 | 4.943 | 0.063 | 4.896 | 0.023 | −24.7 | −10.0 | 0.5 | 86.7 | ab | 1 |
| 80 | 186.11157 | 25.58248 | 5.844 | 0.019 | 5.778 | 0.031 | 5.731 | 0.016 | −9.4 | −10.9 | 0.1 | 85.9 | ab | 1 |
| 81 | 186.12976 | 25.08834 | 14.777 | 0.005 | 14.242 | 0.004 | 13.902 | 0.005 | −21.9 | −21.2 | 0.4 | 90.1 | ce | 3 |
| 82 | 186.18144 | 30.29726 | 11.423 | 0.023 | 10.801 | 0.028 | 10.601 | 0.022 | −11.7 | −10.3 | 0.1 | 85.3 | c | 1 |
| 83 | 186.25937 | 25.56064 | 7.051 | 0.018 | 6.849 | 0.016 | 6.762 | 0.031 | −12.6 | −8.2 | 0.1 | 87.1 | abcf | 1 |
| 84 | 186.26095 | 26.71060 | 11.621 | 0.019 | 11.028 | 0.016 | 10.791 | 0.020 | −11.3 | −8.8 | 0.1 | 84.0 | bc | 1 |
| 85 | 186.34369 | 23.22904 | 7.644 | 0.024 | 7.480 | 0.027 | 7.392 | 0.018 | −11.2 | −10.8 | 0.1 | 86.5 | abf | 1 |
| 86 | 186.35434 | 23.84796 | 10.715 | 0.020 | 10.072 | 0.020 | 9.873 | 0.017 | −11.9 | −7.6 | 0.1 | 89.2 | c | 1 |
| 87 | 186.46641 | 26.77665 | 7.411 | 0.024 | 7.303 | 0.059 | 7.205 | 0.026 | −13.4 | −8.6 | 0.1 | 86.3 | abcf | 1 |
| 88 | 186.47588 | 26.86073 | 11.984 | 0.022 | 11.389 | 0.028 | 11.143 | 0.020 | −11.5 | −7.8 | 0.1 | 87.7 | c | 1 |
| 89 | 186.50104 | 24.15579 | 10.979 | 0.021 | 10.356 | 0.029 | 10.142 | 0.025 | −11.6 | −6.6 | 0.1 | 86.7 | bc | 1 |
| 90 | 186.53527 | 24.65868 | 11.863 | 0.021 | 11.279 | 0.030 | 11.026 | 0.025 | −11.8 | −9.3 | 0.1 | 83.5 | c | 1 |
| 91 | 186.60021 | 27.26820 | 4.409 | 0.240 | 4.235 | 0.194 | 4.149 | 0.036 | −16.0 | −13.4 | 0.5 | 81.6 | ab | 1 |
| 92 | 186.66775 | 27.31204 | 12.462 | 0.022 | 11.896 | 0.029 | 11.672 | 0.025 | −13.5 | −9.2 | 0.2 | 81.8 | c | 1 |
| 93 | 186.71256 | 26.26715 | 9.855 | 0.022 | 9.275 | 0.026 | 9.156 | 0.020 | −12.1 | −8.0 | 0.1 | 86.0 | bcdf | 1 |
| 94 | 186.73599 | 22.67396 | 11.556 | 0.020 | 10.951 | 0.022 | 10.715 | 0.017 | −11.0 | −8.3 | 0.1 | 87.4 | c | 1 |
| 95 | 186.74702 | 26.82568 | 4.796 | 0.192 | 4.727 | 0.020 | 4.649 | 0.024 | −11.5 | −9.2 | 0.6 | 85.7 | ab | 1 |
| 96 | 186.76784 | 25.68371 | 13.946 | 0.030 | 13.395 | 0.040 | 13.026 | 0.030 | −13.6 | −5.9 | 1.1 | 100.0 | c | 1 |
| 97 | 186.77604 | 26.84567 | 8.642 | 0.037 | 8.327 | 0.026 | 8.246 | 0.036 | −12.9 | −7.8 | 0.3 | 89.6 | abcf | 1 |
| 98 | 186.83616 | 23.32981 | 8.912 | 0.021 | 8.537 | 0.021 | 8.451 | 0.017 | −12.4 | −9.1 | 0.1 | 84.0 | bcf | 1 |
| 99 | 186.90981 | 25.91208 | 6.285 | 0.023 | 6.222 | 0.027 | 6.226 | 0.017 | −12.2 | −9.3 | 0.1 | 84.4 | abf | 1 |
| 100 | 186.95118 | 28.19438 | 8.436 | 0.023 | 8.050 | 0.046 | 8.050 | 0.023 | −13.4 | −9.4 | 0.1 | 81.8 | bcf | 1 |
| 101 | 187.01885 | 24.35210 | 12.392 | 0.023 | 11.835 | 0.032 | 11.579 | 0.021 | −12.0 | −9.3 | 0.1 | 84.3 | bc | 1 |
| 102 | 187.03613 | 24.96473 | 12.507 | 0.026 | 11.903 | 0.031 | 11.666 | 0.023 | −3.3 | −17.7 | 0.1 | 100.0 | | 1 |
| 103 | 187.08792 | 28.04054 | 8.943 | 0.024 | 8.472 | 0.044 | 8.465 | 0.027 | −12.7 | −9.0 | 0.1 | 83.2 | bcf | 1 |
| 104 | 187.11487 | 28.56222 | 12.284 | 0.022 | 11.709 | 0.028 | 11.471 | 0.023 | −12.8 | −8.4 | 0.1 | 86.3 | c | 1 |
| 105 | 187.14427 | 29.54501 | 14.337 | 0.004 | 13.835 | 0.003 | 13.467 | 0.003 | −12.1 | −8.8 | 0.3 | 85.3 | c | 3 |
| 106 | 187.15893 | 26.22693 | 6.137 | 0.052 | 6.022 | 0.029 | 5.994 | 0.017 | −7.8 | −10.2 | 0.2 | 86.4 | abf | 1 |
| 107 | 187.18560 | 25.89926 | 6.165 | 0.026 | 6.100 | 0.024 | 6.056 | 0.023 | −22.3 | −17.1 | 0.2 | 73.3 | ab | 1 |
| 108 | 187.22784 | 25.91280 | 5.221 | 0.020 | 5.297 | 0.034 | 5.289 | 0.017 | −23.5 | −15.6 | 0.4 | 73.9 | ab | 1 |
| 109 | 187.23505 | 26.54925 | 9.208 | 0.026 | 8.768 | 0.031 | 8.661 | 0.023 | −12.9 | −9.2 | 0.1 | 84.3 | bcd | 1 |
| 110 | 187.24021 | 27.78009 | 10.989 | 0.023 | 10.349 | 0.028 | 10.185 | 0.022 | −13.8 | −4.9 | 0.1 | 105.7 | bc | 1 |
| 111 | 187.33392 | 24.74286 | 13.553 | 0.026 | 12.984 | 0.032 | 12.679 | 0.021 | −12.3 | −8.4 | 0.2 | 82.0 | c | 1 |
| 112 | 187.33491 | 28.43433 | 13.025 | 0.023 | 12.426 | 0.033 | 12.214 | 0.020 | −12.0 | −8.4 | 0.2 | 89.9 | c | 1 |
| 113 | 187.35376 | 21.78045 | 10.714 | 0.023 | 10.048 | 0.028 | 9.881 | 0.021 | −12.1 | −9.8 | 0.1 | 82.5 | | 1 |
| 114 | 187.42048 | 24.52071 | 8.202 | 0.019 | 7.841 | 0.047 | 7.725 | 0.029 | −11.2 | −8.6 | 0.1 | 87.9 | abcf | 1 |
| 115 | 187.52024 | 24.04274 | 11.774 | 0.022 | 11.182 | 0.016 | 10.937 | 0.019 | −12.0 | −8.7 | 0.1 | 88.0 | bc | 1 |
| 116 | 187.69229 | 23.76363 | 12.718 | 0.024 | 12.167 | 0.030 | 11.910 | 0.022 | −14.7 | −9.8 | 0.1 | 110.0 | b | 1 |
| 117 | 187.73906 | 22.77080 | 11.245 | 0.021 | 10.645 | 0.029 | 10.420 | 0.021 | −12.4 | −9.3 | 0.1 | 82.5 | bc | 1 |
| 118 | 187.75230 | 24.56715 | 5.293 | 0.037 | 5.308 | 0.027 | 5.269 | 0.017 | −12.4 | −9.7 | 0.4 | 83.4 | ab | 1 |
| 119 | 187.76286 | 27.73031 | 7.612 | 0.019 | 7.463 | 0.055 | 7.404 | 0.018 | −12.4 | −8.6 | 0.1 | 86.2 | abcf | 1 |
| 120 | 187.78398 | 24.27641 | 14.402 | 0.004 | 13.869 | 0.003 | 13.460 | 0.003 | −14.0 | −8.4 | 0.4 | 83.7 | c | 3 |
| 121 | 187.86551 | 25.39438 | 11.438 | 0.023 | 10.842 | 0.030 | 10.634 | 0.020 | −12.0 | −8.6 | 0.1 | 84.0 | bc | 1 |
| 122 | 187.90212 | 24.87421 | 13.452 | 0.026 | 12.878 | 0.028 | 12.594 | 0.025 | −11.8 | −9.0 | 0.2 | 86.6 | ce | 1 |
| 123 | 187.96062 | 29.31413 | 6.847 | 0.027 | 6.745 | 0.057 | 6.654 | 0.020 | −10.9 | −6.2 | 0.1 | 83.6 | bf | 1 |

**Table 2**
(Continued)

| No. (1) | R.A. (2000) (deg) (2) | Decl. (2000) (deg) (3) | $J$ (mag) (4) | Jerr (mag) (5) | $H$ (mag) (6) | Herr (mag) (7) | $Ks$ (mag) (8) | Kserr (mag) (9) | $\mu_\alpha \cos \delta$ mas yr$^{-1}$ (10) | $\mu_\delta$ mas yr$^{-1}$ (11) | $\Delta\mu$ mas yr$^{-1}$ (12) | Dist (pc) (13) | Ref.[a] (14) | Data[b] (15) |
|---|---|---|---|---|---|---|---|---|---|---|---|---|---|---|
| 124 | 188.18704 | 23.41905 | 6.836 | 0.029 | 6.720 | 0.044 | 6.659 | 0.020 | 3.7 | −3.1 | 0.1 | 104.2 | | 1 |
| 125 | 188.25256 | 27.71240 | 9.470 | 0.030 | 8.940 | 0.030 | 8.866 | 0.018 | −13.0 | −9.9 | 0.1 | 82.3 | bcdf | 1 |
| 126 | 188.33335 | 22.40649 | 8.855 | 0.019 | 8.470 | 0.023 | 8.402 | 0.020 | −10.3 | −7.4 | 0.1 | 83.9 | cf | 1 |
| 127 | 188.36980 | 26.44913 | 15.029 | 0.006 | 14.500 | 0.005 | 14.236 | 0.007 | −20.6 | −6.0 | 1.1 | 101.0 | | 3 |
| 128 | 188.39255 | 24.28296 | 6.032 | 0.030 | 5.988 | 0.031 | 5.989 | 0.026 | −11.9 | −9.0 | 0.1 | 86.7 | abf | 1 |
| 129 | 188.42545 | 25.94274 | 9.031 | 0.029 | 8.601 | 0.036 | 8.584 | 0.020 | −16.4 | −9.7 | 0.1 | 90.2 | cf | 1 |
| 130 | 188.46503 | 31.11809 | 15.593 | 0.007 | 15.048 | 0.007 | 14.545 | 0.007 | −11.3 | −8.6 | 0.9 | 86.3 | | 3 |
| 131 | 188.63078 | 25.75006 | 10.249 | 0.019 | 9.577 | 0.027 | 9.395 | 0.020 | −13.2 | −9.3 | 0.4 | 84.3 | c | 1 |
| 132 | 188.68958 | 27.38686 | 14.217 | 0.003 | 13.703 | 0.002 | 13.324 | 0.004 | −12.9 | −9.4 | 0.2 | 81.5 | c | 3 |
| 133 | 188.71789 | 25.15673 | 10.893 | 0.023 | 10.289 | 0.028 | 10.058 | 0.020 | −16.7 | −7.3 | 0.3 | 87.5 | c | 1 |
| 134 | 188.72619 | 27.45559 | 7.897 | 0.029 | 7.583 | 0.040 | 7.510 | 0.020 | −16.6 | −10.0 | 0.6 | 120.0 | bc | 1 |
| 135 | 188.82267 | 24.46504 | 11.142 | 0.023 | 10.508 | 0.028 | 10.309 | 0.022 | −11.7 | −7.8 | 0.1 | 89.9 | c | 1 |
| 136 | 188.89199 | 25.01716 | 13.446 | 0.027 | 12.882 | 0.032 | 12.621 | 0.026 | −12.3 | −8.4 | 0.2 | 84.8 | c | 1 |
| 137 | 188.96796 | 27.84477 | 13.851 | 0.027 | 13.228 | 0.032 | 12.955 | 0.028 | −11.8 | −8.5 | 0.2 | 88.3 | | 1 |
| 138 | 189.03665 | 29.80297 | 12.371 | 0.022 | 11.759 | 0.029 | 11.535 | 0.021 | −11.4 | −10.3 | 0.2 | 84.5 | c | 1 |
| 139 | 189.31846 | 30.06635 | 15.147 | 0.006 | 14.630 | 0.006 | 14.276 | 0.006 | −2.7 | 5.3 | 0.4 | 119.8 | | 3 |
| 140 | 189.48458 | 25.86257 | 11.491 | 0.024 | 10.893 | 0.033 | 10.684 | 0.021 | −12.7 | −9.0 | 0.1 | 85.6 | c | 1 |
| 141 | 189.54769 | 23.55611 | 10.776 | 0.022 | 10.163 | 0.023 | 9.963 | 0.020 | −12.0 | −10.3 | 0.1 | 87.3 | | 1 |
| 142 | 189.69180 | 26.31618 | 13.257 | 0.026 | 12.625 | 0.032 | 12.393 | 0.024 | −12.2 | −8.6 | 0.2 | 89.1 | c | 1 |
| 143 | 190.19120 | 27.20596 | 12.407 | 0.029 | 11.849 | 0.032 | 11.586 | 0.024 | −12.8 | −8.5 | 0.1 | 85.4 | c | 1 |
| 144 | 190.66186 | 25.16037 | 11.298 | 0.020 | 10.689 | 0.021 | 10.460 | 0.018 | −11.3 | −7.5 | 0.1 | 90.3 | c | 1 |
| 145 | 190.77738 | 24.25476 | 12.240 | 0.020 | 11.653 | 0.021 | 11.414 | 0.018 | −12.2 | −8.6 | 0.1 | 84.3 | c | 1 |
| 146 | 190.86251 | 23.99538 | 8.207 | 0.021 | 7.895 | 0.021 | 7.853 | 0.021 | 0.7 | −4.2 | 0.1 | 88.3 | | 1 |
| 147 | 190.89413 | 23.43523 | 13.495 | 0.003 | 12.957 | 0.002 | 12.684 | 0.002 | −3.4 | 1.0 | 0.1 | 105.6 | | 3 |
| 148 | 191.06186 | 23.45737 | 12.623 | 0.002 | 12.186 | 0.001 | 11.840 | 0.001 | −25.8 | −7.4 | 0.1 | 106.3 | | 3 |
| 149 | 191.12490 | 24.93406 | 11.262 | 0.022 | 10.696 | 0.030 | 10.452 | 0.021 | −12.2 | −8.8 | 0.1 | 82.5 | | 1 |
| 150 | 191.12880 | 28.16368 | 12.242 | 0.024 | 11.655 | 0.030 | 11.417 | 0.024 | −12.7 | −8.9 | 0.1 | 83.1 | c | 1 |
| 151 | 191.13160 | 25.78914 | 14.649 | 0.004 | 14.143 | 0.004 | 13.722 | 0.004 | −12.2 | −7.8 | 0.4 | 82.6 | | 3 |
| 152 | 191.67721 | 25.40008 | 13.938 | 0.027 | 13.351 | 0.031 | 13.027 | 0.037 | −11.9 | −7.2 | 0.2 | 87.4 | c | 1 |
| 153 | 191.69063 | 24.98089 | 14.612 | 0.004 | 14.116 | 0.003 | 13.777 | 0.004 | −7.4 | −3.3 | 0.9 | 102.3 | | 3 |
| 154 | 191.84451 | 24.76349 | 15.117 | 0.006 | 14.628 | 0.004 | 14.196 | 0.006 | −11.8 | −9.3 | 0.6 | 81.9 | | 3 |
| Distance by *phot-d* | | | | | | | | | | | | | | |
| 155 | 181.54707 | 26.83880 | 16.320 | 0.013 | 15.755 | 0.011 | 15.313 | 0.015 | −14.8 | −6.4 | 3.2 | 115.8 | | 4 |
| 156 | 182.06965 | 27.51282 | 12.312 | 0.001 | 11.709 | 0.001 | 11.359 | 0.001 | 0.3 | −11.4 | 2.8 | 104.6 | | 4 |
| 157 | 182.16738 | 26.29052 | 16.088 | 0.011 | 15.486 | 0.008 | 15.078 | 0.013 | −13.7 | −23.5 | 3.2 | 109.7[c] | | 4 |
| 158 | 182.76838 | 26.46638 | 14.833 | 0.005 | 14.242 | 0.003 | 13.918 | 0.004 | −25.2 | −8.1 | 2.9 | 99.2[c] | | 4 |
| 159 | 182.81209 | 23.59442 | 16.787 | 0.020 | 16.109 | 0.013 | 15.499 | 0.014 | −2.2 | −9.1 | 6.9 | 87.1[c] | | 4 |
| 160 | 183.35818 | 21.50937 | 16.082 | 0.009 | 15.466 | 0.010 | 15.064 | 0.011 | −17.5 | −3.3 | 3.5 | 109.1[c] | | 4 |
| 161 | 183.48757 | 25.08627 | 9.797 | 0.020 | 9.130 | 0.014 | 9.071 | 0.013 | −8.8 | 1.4 | 5.1 | 103.0[c] | | 2 |
| 162 | 183.67470 | 26.49705 | 9.724 | 0.020 | 9.068 | 0.015 | 8.925 | 0.016 | 0.7 | 1.1 | 5.1 | 79.4[c] | | 2 |
| 163 | 184.51479 | 23.83123 | 10.725 | 0.022 | 10.054 | 0.020 | 9.938 | 0.018 | −4.1 | −6.7 | 5.2 | 116.0[c] | | 2 |
| 164 | 184.55135 | 29.10878 | 10.232 | 0.022 | 9.540 | 0.022 | 9.396 | 0.020 | −5.0 | −10.7 | 5.5 | 76.7[c] | | 2 |
| 165 | 184.60960 | 26.96763 | 12.921 | 0.029 | 12.329 | 0.036 | 12.070 | 0.022 | −23.0 | −17.5 | 5.9 | 80.2 | | 2 |
| 166 | 184.61984 | 30.78003 | 10.680 | 0.026 | 9.980 | 0.030 | 9.844 | 0.022 | −7.4 | −12.8 | 6.0 | 99.3[c] | | 2 |
| 167 | 185.20981 | 22.08020 | 13.441 | 0.046 | 12.778 | 0.044 | 12.551 | 0.041 | −24.5 | −11.8 | 5.2 | 105.7 | | 2 |
| 168 | 185.21537 | 23.32075 | 12.586 | 0.021 | 12.016 | 0.023 | 11.765 | 0.020 | −1.8 | −4.7 | 5.3 | 107.9 | | 2 |
| 169 | 185.25005 | 21.91837 | 9.638 | 0.022 | 9.040 | 0.024 | 8.870 | 0.017 | −1.2 | −6.8 | 5.2 | 72.6[c] | | 2 |
| 170 | 185.31003 | 21.17550 | 10.633 | 0.021 | 9.910 | 0.022 | 9.780 | 0.018 | −8.5 | −1.7 | 5.2 | 111.5[c] | c | 2 |
| 171 | 185.37505 | 23.18350 | 15.490 | 0.007 | 14.930 | 0.005 | 14.608 | 0.007 | −5.5 | −2.4 | 3.4 | 92.0[c] | | 4 |
| 172 | 185.55564 | 21.48469 | 14.834 | 0.005 | 14.265 | 0.004 | 13.937 | 0.005 | −4.1 | −15.9 | 3.4 | 67.9[c] | | 4 |
| 173 | 185.71817 | 26.64010 | 9.777 | 0.027 | 9.263 | 0.032 | 9.115 | 0.021 | −9.4 | 2.7 | 5.8 | 91.0 | bc | 2 |
| 174 | 185.74752 | 24.98287 | 9.396 | 0.027 | 8.811 | 0.044 | 8.674 | 0.019 | −13.8 | −7.9 | 5.8 | 96.8[c] | cd | 2 |
| 175 | 185.79713 | 25.56805 | 10.430 | 0.018 | 9.735 | 0.016 | 9.591 | 0.019 | −0.9 | −6.9 | 5.1 | 102.2[c] | | 2 |
| 176 | 185.98912 | 24.89141 | 16.065 | 0.012 | 15.433 | 0.009 | 14.927 | 0.012 | −17.1 | −6.0 | 3.3 | 75.5[c] | e | 4 |
| 177 | 186.69448 | 23.61378 | 10.303 | 0.022 | 9.645 | 0.020 | 9.514 | 0.017 | −14.5 | −17.9 | 5.2 | 117.6[c] | | 2 |
| 178 | 186.85393 | 26.22864 | 10.770 | 0.024 | 9.999 | 0.029 | 9.860 | 0.020 | −8.1 | −5.7 | 5.9 | 106.1[c] | | 2 |
| 179 | 187.63748 | 30.36935 | 12.303 | 0.001 | 11.663 | 0.001 | 11.439 | 0.001 | −17.6 | −12.1 | 2.5 | 111.8 | | 4 |
| 180 | 187.83843 | 30.44276 | 13.445 | 0.023 | 12.906 | 0.030 | 12.623 | 0.021 | −11.9 | −9.4 | 5.5 | 109.4 | | 2 |
| 181 | 187.89421 | 24.09135 | 11.948 | 0.021 | 11.318 | 0.028 | 11.091 | 0.021 | −21.1 | −19.2 | 6.0 | 51.1 | | 2 |
| 182 | 188.02089 | 24.15844 | 15.424 | 0.006 | 14.866 | 0.006 | 14.653 | 0.010 | 1.9 | −14.2 | 3.2 | 98.3[c] | | 4 |
| 183 | 188.33619 | 24.95474 | 10.794 | 0.030 | 10.123 | 0.032 | 9.927 | 0.020 | −16.5 | −16.6 | 5.9 | 52.8 | c | 2 |

**Table 2**
(Continued)

| No. (1) | R.A. (2000) (deg) (2) | Decl. (2000) (deg) (3) | $J$ (mag) (4) | Jerr (mag) (5) | $H$ (mag) (6) | Herr (mag) (7) | $Ks$ (mag) (8) | Kserr (mag) (9) | $\mu_\alpha \cos\delta$ mas yr$^{-1}$ (10) | $\mu_\delta$ mas yr$^{-1}$ (11) | $\Delta\mu$ mas yr$^{-1}$ (12) | Dist (pc) (13) | Ref.[a] (14) | Data[b] (15) |
|---|---|---|---|---|---|---|---|---|---|---|---|---|---|---|
| 184 | 189.06597 | 23.41478 | 13.492 | 0.002 | 12.995 | 0.002 | 12.636 | 0.002 | −8.3 | 1.9 | 3.0 | 71.4 | | 4 |
| 185 | 189.07309 | 22.65018 | 9.640 | 0.020 | 9.069 | 0.031 | 8.882 | 0.014 | −11.2 | −7.4 | 5.5 | 88.8[c] | | 2 |
| 186 | 189.35725 | 27.17839 | 10.385 | 0.022 | 9.708 | 0.028 | 9.603 | 0.021 | −6.1 | −4.1 | 5.9 | 109.5[c] | | 2 |
| 187 | 189.80086 | 23.18844 | 13.490 | 0.023 | 12.866 | 0.022 | 12.602 | 0.024 | −25.0 | −14.2 | 4.9 | 102.3[c] | | 2 |
| 188 | 190.22918 | 23.83889 | 10.011 | 0.021 | 9.316 | 0.019 | 9.162 | 0.017 | −5.4 | −16.1 | 4.9 | 92.8[c] | | 2 |
| 189 | 190.37988 | 23.67833 | 15.170 | 0.006 | 14.673 | 0.004 | 14.304 | 0.006 | −4.9 | −3.2 | 3.4 | 117.8 | | 4 |
| 190 | 190.41708 | 26.93449 | 8.852 | 0.018 | 8.346 | 0.038 | 8.278 | 0.020 | −14.0 | 7.4 | 5.8 | 68.9 | | 2 |
| 191 | 190.72371 | 24.91863 | 17.530 | 0.035 | 16.688 | 0.025 | 15.963 | 0.028 | −16.6 | −1.6 | 3.7 | 61.4 | | 4 |
| 192 | 191.40753 | 24.84447 | 15.569 | 0.008 | 15.070 | 0.006 | 14.696 | 0.009 | 2.0 | −11.9 | 3.2 | 95.9[c] | | 4 |

**Notes.**
[a] (a) Trumpler (1938), (b) Casewell et al. (2006), (c) Kraus & Hillenbrand (2007), (d) Mermilliod et al. (2008), (e) Melnikov & Eislöffel (2012), (f) Gaia Collaboration et al. (2017), (g) Casewell et al. (2005).
[b] (1) 2MASS photometry and *Gaia*/DR2 proper motions, (2) 2MASS photometry and URAT-1 proper motions, (3) UKIDSS/GCS photometry and *Gaia*/DR2 proper motions, (4) both photometry and proper motions are from UKIDSS/GCS.
[c] *Gaia*/DR2 parallax measurements with $\varpi/\Delta\varpi < 10$.

(This table is available in machine-readable form.)

**Table 3**
Selected Literature Members beyond the 5° Radius Confirmed by This Work

| No. (1) | R.A. (2000) (deg) (2) | Decl. (2000) (deg) (3) | $J$ (mag) (4) | Jerr (mag) (5) | $H$ (mag) (6) | Herr (mag) (7) | $Ks$ (mag) (8) | Kserr (mag) (9) | $\mu_\alpha \cos\delta$ mas yr$^{-1}$ (10) | $\mu_\delta$ mas yr$^{-1}$ (11) | $\Delta\mu$ mas yr$^{-1}$ (12) | Dist (pc) (13) | Ref.[a] (14) |
|---|---|---|---|---|---|---|---|---|---|---|---|---|---|
| 1 | 177.15700 | 28.27510 | 9.02 | 0.026 | 8.63 | 0.029 | 8.59 | 0.02 | −12.06 | −9.36 | 0.09 | 89.29 | f |
| 2 | 178.88890 | 29.72820 | 9.69 | 0.022 | 9.19 | 0.022 | 9.06 | 0.017 | −15.71 | −9.67 | 0.11 | 90.45 | f |
| 3 | 179.31637 | 24.65142 | 12.05 | 0.024 | 11.44 | 0.024 | 11.2 | 0.023 | −12.32 | −10.85 | 0.14 | 84.31 | c |
| 4 | 179.72550 | 23.85242 | 12.21 | 0.02 | 11.65 | 0.024 | 11.38 | 0.018 | −11.75 | −8.79 | 0.17 | 91.18 | c |
| 5 | 179.77171 | 26.74294 | 11.22 | 0.019 | 10.58 | 0.019 | 10.37 | 0.019 | −12.02 | −8.79 | 0.06 | 89.33 | c |
| 6 | 180.61090 | 20.12300 | 8.65 | 0.018 | 8.39 | 0.034 | 8.31 | 0.02 | −12.14 | −7.95 | 0.08 | 90.26 | f |
| 7 | 184.47371 | 20.37667 | 12.33 | 0.021 | 11.72 | 0.022 | 11.5 | 0.018 | −13.98 | −8.02 | 0.30 | 82.26 | c |
| 8 | 184.62110 | 32.74890 | 6.13 | 0.019 | 6.05 | 0.024 | 6.02 | 0.016 | −13.01 | −9.28 | 0.13 | 83.66 | f |
| 9 | 188.12946 | 35.33119 | 8.41 | 0.019 | 8.13 | 0.023 | 8.09 | 0.018 | −12.22 | −10.34 | 0.07 | 83.61 | df |
| 10 | 188.52692 | 32.02686 | 7.28 | 0.02 | 7.06 | 0.02 | 7.02 | 0.023 | −10.17 | −11.71 | 0.08 | 120.14 | c |
| 11 | 191.77800 | 22.61680 | 7.32 | 0.032 | 7.08 | 0.038 | 7.03 | 0.017 | −12.59 | −8.92 | 0.10 | 83.30 | f |
| 12 | 192.92465 | 27.54068 | 3.629 | 0.292 | 3.367 | 0.218 | 3.26 | 0.286 | −10.99 | −8.31 | 0.34 | 87.01 | bd |
| 13 | 193.04837 | 25.37350 | 7.88 | 0.021 | 7.65 | 0.021 | 7.61 | 0.015 | −11.47 | −8.55 | 0.08 | 85.13 | cdf |
| 14 | 194.40350 | 28.97910 | 8.9 | 0.026 | 8.54 | 0.046 | 8.47 | 0.02 | −11.57 | −5.35 | 0.10 | 91.74 | f |
| 15 | 195.14658 | 23.65175 | 7.38 | 0.021 | 7.22 | 0.018 | 7.18 | 0.02 | −11.97 | −8.88 | 0.11 | 86.15 | df |

**Note.**
[a] (a) Trumpler (1938), (b) Casewell et al. (2006), (c) Kraus & Hillenbrand (2007), (d) Mermilliod et al. (2008), (e) Melnikov & Eislöffel (2012), (f) Gaia Collaboration et al. (2017).

data taken with TripleSpec, which includes the pre-processing, aperture extraction, and wavelength calibrations. The individual extracted and wavelength-calibrated spectra from a given sequence of observations, each with their own A0 standard star, were then scaled to a common median flux and combined using XCOMBSPEC in SPEXTOOL. The combined spectra were corrected for telluric absorption and flux-calibrated using the respective telluric standards with XTELLCOR. All calibrated sets of observations of a given target were then median-combined to produce the final spectrum.

The spectra of candidates No. 191 and 160 were acquired by Gemini Fast Turnaround GN-2017B-FT-18, on 7 and on 11 December 2017, respectively, both under good sky conditions, using the cross-dispersed mode of GNIRS (Elias et al. 2006a, 2006b), covering 0.9–2.5 $\mu$m simultaneously with a resolving power $R \sim 1200$. The short blue camera with 32 lines/mm grating was selected with a slit width 0.″45 for No. 191 and 0.″675 for No. 160. The individual exposure time under the A-B-B-A nodding sequence was 150 s for No. 191, and 60 s for No. 160. Three sets of nodding sequence were observed for No. 191, and one set was taken for No. 160.

The GNIRS raw data were reduced by PyRAF using the Gemini and GRNIRS packages. We first cleaned the pattern noise, radiation events, flat-field, and sky-subtraction, then did the wavelength calibration by spectra of arc lamps. Each spectrum was extracted from the combined ABBA exposure files. Telluric absorption lines were removed with two A2 V standard stars (HIP 58297 and HIP 63006) observed before or after the observing run.

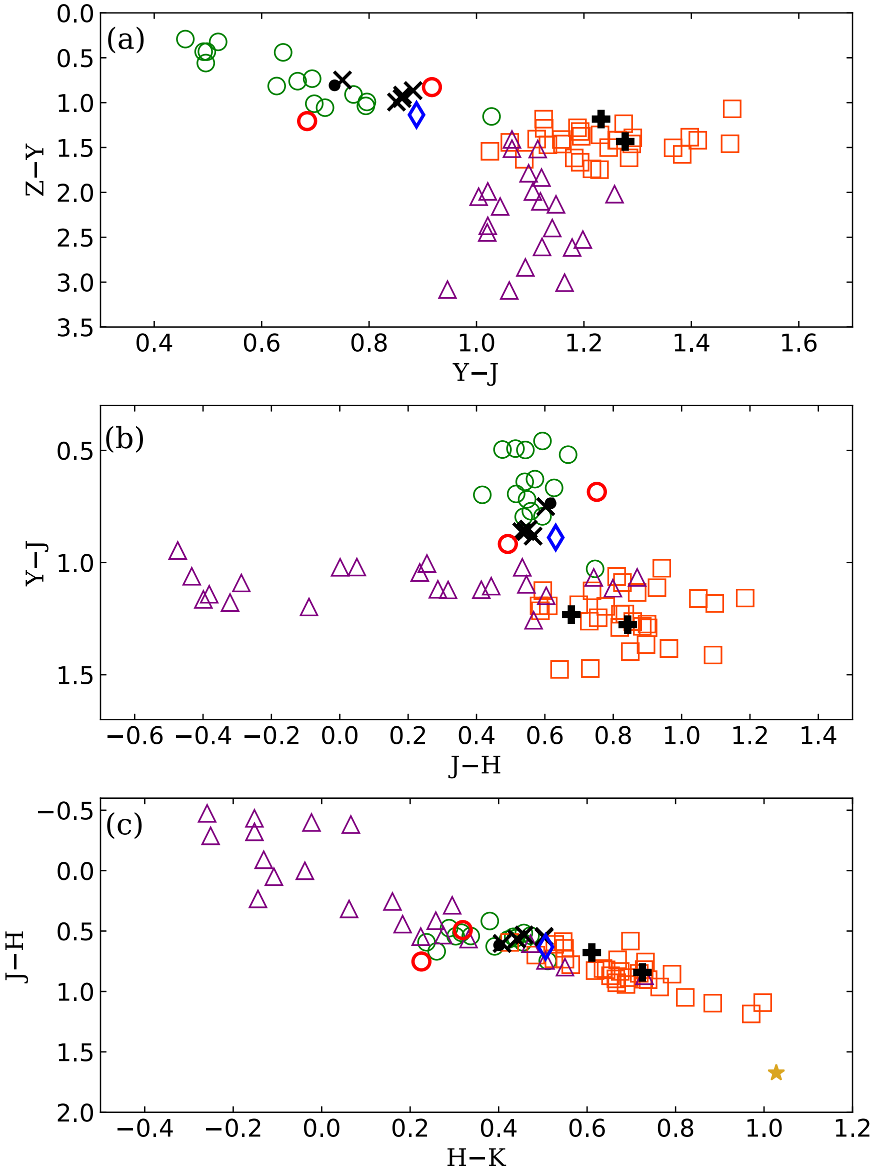


**Figure 11.** UKIDSS two-color diagrams of the M (green open circles), L (orange open squares), and T (purple open triangles) dwarfs in Hewett et al. (2006) in (a) $(Z-Y)$ vs. $(Y-J)$, (b) $(Y-J)$ vs. $(J-H)$, and (c) $(J-H)$ vs. $(H-K)$ diagrams. The known M dwarfs from West et al. (2011) (i.e., our Nos. 6, 55, 130, 155, and 157) are represented by black crosses; the M9 reported by Casewell et al. (2014; our No. 176) is marked as a blue diamond. The M brown dwarf and two L dwarfs found by this work are in black filled circles and in black pluses. Objects A and B are shown as thick red open circles, whereas object C, having no $Z$ or $Y$ detection, is marked with a golden star symbol.

Each reduced Palomar or Gemini 1D spectrum was then compared with the low-dispersion template spectra of brown dwarfs from SpeX (Rayner et al. 2003), from which the "best" match, judged by eye examination, was determined. Three candidates turned out to be bona fide substellar objects, with one late-M (No. 160), one early-L (No. 159), and one mid-L type (No. 191), shown in Figure 13. The classification was warranted by the characteristic absorption features due to methane/water near 1.4 $\mu$m.

The Palomar/TripleSpec spectra for objects A and B are exhibited in Figure 14, together with template spectra from SpeX. Both spectra show the CN band feature near 1.1 $\mu$m characteristic of giants and supergiants (Loidl et al. 2001; Lançon et al. 2007). The *Gaia* measurements, however, yield $\varpi = 2.5 \pm 0.2$ mas for star A, and $\varpi = 2.6 \pm 0.3$ mas for star B, respectively, placing each at $\sim$400 pc. Their optical brightness ($g_{P1} \sim 20$ mag) is hence consistent more with M dwarfs ($M_V = 9$–$10$ mag) than with giants ($M_V \sim -0.3$) (Cox 2000). Further spectroscopic observations are required to provide information on the nature of these two stars, such as, for example, whether they belong to the dwarf carbon population. In any case, neither of them is associated with the cluster.

## 4. Discussion

### 4.1. Age of Coma Ber

The age we derive for Coma Ber, $\sim$800 Myr, is based on the consistency of evolved members with model isochrones (see Section 3.1), for which no rotation is taken into account. Rotation affects the equations of stellar structure, and with elevated centrifugal force, acts to reduce the stellar mass,

**Table 4**
Brown Dwarf Members of Coma Ber and Miscellaneous Objects

| No. | R.A. (deg) | Decl. (deg) | $Z$ (mag) | $Y$ (mag) | $J$ (mag) | $H$ (mag) | $K1$ (mag) | $\mu_\alpha \cos\delta$ (mas yr$^{-1}$) | $\mu_\delta$ (mas yr$^{-1}$) | Spectroscopy (SpT) | *photo-type* (SpT) |
|---|---|---|---|---|---|---|---|---|---|---|---|
| | | | | | Brown Dwarf Members | | | | | | |
| 6 | 181.39774 | +25.02538 | 17.3756 | 16.3825 | 15.5315 | 14.9799 | 14.4771 | −12.9 | −9.9 | M8[a] | M7 |
| 155 | 181.54707 | +26.83880 | 18.0680 | 17.2021 | 16.3201 | 15.7545 | 15.3133 | −11.3 | −5.8 | M8[a] | M7 |
| 157 | 182.16738 | +26.29052 | 17.5872 | 16.8390 | 16.0885 | 15.4859 | 15.0781 | −10.2 | −22.9 | M8[a] | M7 |
| 176 | 185.98912 | +24.89141 | 18.0889 | 16.9529 | 16.0646 | 15.4329 | 14.9268 | −13.5 | −5.3 | M9[b] | M9 |
| 55 | 185.42258 | +21.68386 | 17.4297 | 16.5134 | 15.6511 | 15.1188 | 14.6610 | −10.6 | −8.2 | M9[a] | M7 |
| 130 | 188.46503 | +31.11809 | 17.4072 | 16.4539 | 15.5926 | 15.0481 | 14.5452 | −11.3 | −8.6 | M9[a] | M9 |
| 159 | 182.81209 | +23.59442 | 19.2019 | 18.0187 | 16.7868 | 16.1094 | 15.4987 | 1.4 | −8.5 | L2[c] | L2 |
| 160 | 183.35818 | +21.50937 | 17.6250 | 16.8178 | 16.0820 | 15.4655 | 15.0643 | −13.9 | −2.7 | M8[c] | M7 |
| 191 | 190.72371 | +24.91863 | 20.2402 | 18.8068 | 17.5300 | 16.6876 | 15.9625 | −13.0 | −1.0 | L4[c] | L5 |
| | | | | | Miscellaneous Objects | | | | | | |
| A | 183.19468 | +25.50436 | 17.7934 | 16.5876 | 15.9029 | 15.1508 | 14.9253 | −13.0 | 2.1 | MIII? | M1.5 |
| B | 188.90996 | +23.19031 | 17.7026 | 16.8755 | 15.9585 | 15.4668 | 15.1479 | −3.0 | −7.7 | MIII? | M3 |
| C | 186.48545 | +22.78955 | … | … | 19.1199 | 17.4459 | 16.4182 | −7.3 | −4.6 | … | … |

**Notes.**
[a] West et al. (2011).
[b] Casewell et al. (2014).
[c] This work.

thereby prolonging the main-sequence lifetime and core helium burning phase (Kippenhahn et al. 1970). This age is older than the 400–600 Myr often quoted in the literature.

Lithium abundances have been measured for solar-type members in Coma Ber (Jeffries 1999; Ford et al. 2001), particularly in the context of convective mixing in stellar interior in terms of metallicity versus age, e.g., in comparison with stars of similar spectral types in the Hyades and Praesepe, or in the much younger Pleiades (see for example Ford et al. 2001). With an older age, it is not clear if the lithium depletion boundary is still applicable as a chronometer (Martín et al. 2018). In any case, our candidate list contains quite a number of solar-type or cooler members to shed light on the subject.

### 4.2. The Shape and Size of the Cluster

Adopting a distance 85 pc, the angular radius 5° of the cluster corresponds to a linear radius ~7 pc, to be compared with the tidal radius of the cluster 6–7 pc (Casewell et al. 2006; Kraus & Hillenbrand 2007). The Galactic distribution of our candidates, including those in Tables 2 and 3, is illustrated in Figure 15. Given the high Galactic latitude ($\ell \approx +84°$) position of the cluster, the distribution in the $X$–$Y$ plane, i.e., the top view on the Galactic plane, resembles what appears in the celestial sphere, e.g., in R.A. and decl. coordinates, for which members are concentrated within a linear extent about 15 pc n roughly circular shape. The effect of mass segregation is clearly manifest, namely, with more massive members (with larger-sized and lighter-shadowed symbols) concentrating more toward the center. The number of members is markedly reduced beyond a radius of ~10 pc, indicative that the cluster is not more extended as projected in the sky than the sky coverage in our analysis.

However, the situation in the $X$–$Z$ plane, namely the side view of the plane, is different. The apparent cone shape from the bottom upward is the consequence of our pencil-beam view, and the longer extent in the $Z$ direction results from our analysis volume, as we started out with a larger distance range (50–120 pc) to search for candidates than in the angular extent in the sky (within 5° radius of the UKIDSS/GCS coverage). That there are more distant sources beyond ~100 pc than nearby ones closer than ~60 pc is the consequence of the space volume effect, hence many must be false positives. The grouping between $Z \sim$ 65–95 pc represents the cluster, with a linear size twice as extended as in the $X$–$Y$ plane, stretching toward the Galactic plane. Odenkirchen et al. (1998) reported a heliocentric space motion for the cluster $(U, V, W) = (-2.3, -5.5, -0.7)$ km s$^{-1}$ with an error of 0.2 km s$^{-1}$ in each component. As such, the motion of the cluster is primarily along $V$, i.e., in the Galactic rotation, and the cluster is almost at its highest location above the plane. The prolate spheroidal shape is likely the consequence of the tidal pull by the disk.

### 4.3. The Statistical Sample of Members

Analysis of the control field (see Section 3.2) with the same selection criteria led to 14 false positives. Considering the sky area of the control field relative to the cluster region, and assuming the same field distribution toward the cluster region as in the control field, this means out of the 192 candidates, there are roughly 44 field stars that coincidentally share the same ranges of proper motions, distances, and color–magnitude relation as true members, but are not physically associated with the cluster. Additional scrutiny of members against field stars in the same volume would have to rely on metallicity or chemical abundances, e.g., (Ford et al. 2001, by lithium abundances). For the faint sample, no control field is available because of the limit of the UKIDSS/GCS spatial coverage. After field subtraction for the bright sample, plus the entire faint candidate sample, there are 148 members. We emphasize that this is a statistical sample in the sense that out of the 196 candidates, there are 148 true members, but we do not know for sure individually which ones are true members. This is the sample we use to derive member statistics such as the luminosity function, mass function, total stellar mass, etc.

**Table 5**
Literature Candidates Rejected by Our Analysis

| R.A. (deg) | Decl. (deg) | Ref.[a] | Rej.[b] | R.A. (deg) | Decl. (deg) | Ref.[a] | Rej.[b] |
|---|---|---|---|---|---|---|---|
| 181.094000 | 24.021440 | c | 1 | 186.260417 | 26.717778 | e | 1 |
| 181.558040 | 26.780640 | c | 6 | 186.268333 | 23.699444 | e | 1 |
| 181.974620 | 25.929310 | c | 4 | 186.270417 | 25.312500 | e | 5 |
| 182.081080 | 21.082720 | c | 1 | 186.292250 | 27.662440 | bc | 4 |
| 182.301833 | 26.660806 | bc | 4 | 186.388750 | 24.356667 | e | 7 |
| 183.146080 | 27.494080 | c | 5 | 186.391667 | 25.241111 | e | 1 |
| 183.389280 | 27.472287 | g | 7 | 186.482333 | 29.127306 | b | 4 |
| 183.433042 | 27.311437 | g | 5 | 186.517083 | 24.314444 | e | 1 |
| 183.533920 | 22.840920 | c | 4 | 186.522833 | 26.743972 | bc | 6 |
| 183.582417 | 25.179611 | b | 7 | 186.600040 | 25.261940 | c | 6 |
| 183.599875 | 28.354611 | b | 4 | 186.655500 | 22.581500 | b | 4 |
| 183.820542 | 28.747222 | b | 4 | 186.722917 | 25.731944 | e | 1 |
| 183.824362 | 27.919314 | g | 5 | 186.753375 | 29.610528 | b | 2 |
| 183.891708 | 26.261917 | bc | 2 | 186.762917 | 28.546667 | e | 1 |
| 183.955417 | 27.326944 | e | 5 | 186.767917 | 25.682778 | e | 5 |
| 183.980833 | 26.949167 | e | 4 | 186.785667 | 27.023028 | b | 6 |
| 184.010417 | 28.048667 | b | 4 | 186.821250 | 26.355833 | e | 4 |
| 184.079540 | 26.927080 | c | 6 | 186.836565 | 27.169444 | a | 4 |
| 184.086667 | 25.306667 | e | 1 | 186.859500 | 24.782500 | d | 5 |
| 184.095167 | 24.316972 | b | 4 | 186.955184 | 27.991243 | g | 1 |
| 184.121708 | 23.542472 | b | 4 | 186.969417 | 25.095750 | ad | 2 |
| 184.206000 | 24.855861 | d | 5 | 187.027500 | 24.293333 | e | 5 |
| 184.233333 | 25.947778 | e | 1 | 187.042083 | 28.581111 | e | 1 |
| 184.249439 | 27.334819 | g | 1 | 187.067083 | 26.178889 | e | 5 |
| 184.309167 | 25.515278 | e | 3 | 187.106500 | 29.898444 | d | 4 |
| 184.335833 | 25.081667 | e | 1 | 187.114625 | 29.878417 | d | 7 |
| 184.356000 | 27.242310 | c | 2 | 187.142875 | 23.541833 | b | 4 |
| 184.417917 | 24.364444 | e | 5 | 187.157917 | 28.096389 | e | 1 |
| 184.434583 | 25.827778 | e | 1 | 187.161250 | 25.986944 | b | 6 |
| 184.439167 | 27.295556 | e | 1 | 187.181667 | 24.431111 | e | 4 |
| 184.449167 | 28.119722 | e | 5 | 187.188333 | 27.189167 | e | 1 |
| 184.461667 | 23.825278 | e | 5 | 187.208667 | 27.294917 | b | 6 |
| 184.496250 | 26.535000 | e | 3 | 187.270000 | 25.070000 | e | 5 |
| 184.561710 | 21.533000 | c | 4 | 187.305417 | 23.794167 | e | 1 |
| 184.574042 | 23.642444 | b | 4 | 187.362667 | 24.108917 | b | 7 |
| 184.611250 | 25.883560 | c | 1 | 187.375083 | 29.512722 | b | 4 |
| 184.636255 | 27.625217 | g | 7 | 187.417500 | 26.332222 | e | 1 |
| 184.677083 | 24.413333 | e | 1 | 187.425670 | 28.620750 | c | 6 |
| 184.712625 | 26.323444 | d | 1 | 187.436083 | 25.543194 | d | 1 |
| 184.720833 | 27.217222 | e | 1 | 187.558750 | 25.028417 | ad | 1 |
| 184.738625 | 25.886417 | bcd | 4 | 187.559167 | 24.635000 | e | 1 |
| 184.744583 | 26.058583 | cd | 2 | 187.611667 | 24.893611 | e | 1 |
| 184.771583 | 26.184556 | d | 3 | 187.674715 | 28.001458 | g | 7 |
| 184.785500 | 25.053222 | d | 6 | 187.695833 | 26.057500 | e | 5 |
| 184.811040 | 27.930640 | c | 2 | 187.751167 | 26.940306 | b | 4 |
| 184.817750 | 25.436250 | ad | 4 | 187.769917 | 24.262611 | bc | 2 |
| 184.889206 | 24.546867 | g | 7 | 187.855417 | 24.541111 | e | 1 |
| 184.945000 | 27.443611 | e | 1 | 187.964583 | 25.042778 | e | 1 |
| 185.023792 | 25.910222 | d | 4 | 187.989250 | 25.145139 | bc | 4 |
| 185.101250 | 25.139444 | e | 5 | 188.033708 | 28.901806 | bc | 4 |
| 185.112083 | 26.775556 | e | 5 | 188.049285 | 27.115717 | g | 7 |
| 185.131667 | 24.603889 | e | 6 | 188.115000 | 23.765833 | e | 1 |
| 185.150833 | 28.451944 | e | 2 | 188.157500 | 24.656944 | e | 5 |
| 185.151250 | 25.092778 | e | 5 | 188.257500 | 24.654444 | e | 4 |
| 185.185833 | 27.262500 | e | 1 | 188.375792 | 26.166694 | bcd | 4 |
| 185.226250 | 25.432222 | e | 1 | 188.376292 | 28.215528 | b | 4 |
| 185.260153 | 26.367863 | g | 1 | 188.380625 | 24.202528 | b | 5 |
| 185.328735 | 26.708572 | g | 5 | 188.383750 | 24.773056 | e | 5 |
| 185.337125 | 32.176444 | d | 1 | 188.393750 | 24.656111 | e | 1 |
| 185.383750 | 23.754722 | e | 1 | 188.475917 | 27.134639 | cd | 2 |
| 185.582500 | 25.290833 | e | 1 | 188.559250 | 28.378310 | c | 2 |
| 185.607583 | 25.317583 | d | 7 | 188.695542 | 24.160472 | bcd | 2 |
| 185.669375 | 25.669972 | d | 1 | 188.751375 | 30.192667 | d | 1 |

**Table 5**
(Continued)

| R.A. (deg) | Decl. (deg) | Ref.[a] | Rej.[b] | R.A. (deg) | Decl. (deg) | Ref.[a] | Rej.[b] |
|---|---|---|---|---|---|---|---|
| 185.673040 | 27.247560 | ce | 4 | 188.820958 | 26.056056 | b | 5 |
| 185.717670 | 25.066670 | c | 2 | 188.929420 | 25.922970 | c | 2 |
| 185.740000 | 24.809167 | e | 7 | 189.019330 | 27.959890 | c | 2 |
| 185.761667 | 27.645278 | e | 1 | 189.142917 | 25.010639 | b | 5 |
| 185.799958 | 29.249972 | b | 5 | 189.218708 | 24.024194 | d | 3 |
| 185.839710 | 21.712560 | c | 2 | 189.450710 | 26.963110 | c | 2 |
| 185.869580 | 22.848860 | bc | 3 | 189.519667 | 25.855139 | b | 4 |
| 185.880000 | 23.610556 | e | 5 | 189.562250 | 26.357806 | b | 3 |
| 186.020000 | 25.563889 | e | 1 | 189.730667 | 25.893917 | d | 1 |
| 186.043208 | 29.488778 | b | 4 | 189.941250 | 28.299083 | d | 3 |
| 186.070417 | 24.892500 | e | 1 | 189.968458 | 25.775833 | b | 4 |
| 186.071458 | 24.324556 | abcd | 2 | 190.054167 | 28.222500 | d | 1 |
| 186.095625 | 25.915611 | d | 6 | 190.103710 | 27.918310 | c | 4 |
| 186.107540 | 21.604860 | c | 4 | 190.270708 | 25.704972 | d | 4 |
| 186.111040 | 25.752140 | c | 4 | 190.560620 | 28.603560 | c | 6 |
| 186.223333 | 23.718028 | bc | 4 | 190.854460 | 26.785470 | c | 4 |

**Notes.**
[a] (a) Trumpler (1938), (b) Casewell et al. (2006), (c) Kraus & Hillenbrand (2007), (d) Mermilliod et al. (2008), (e) Melnikov & Eislöffel (2012), (f) Gaia Collaboration et al. (2017), (g) Casewell et al. (2005).
[b] (1) Rejection by proper motion, (2) rejection by CMD, (4) rejection by distance (additive).

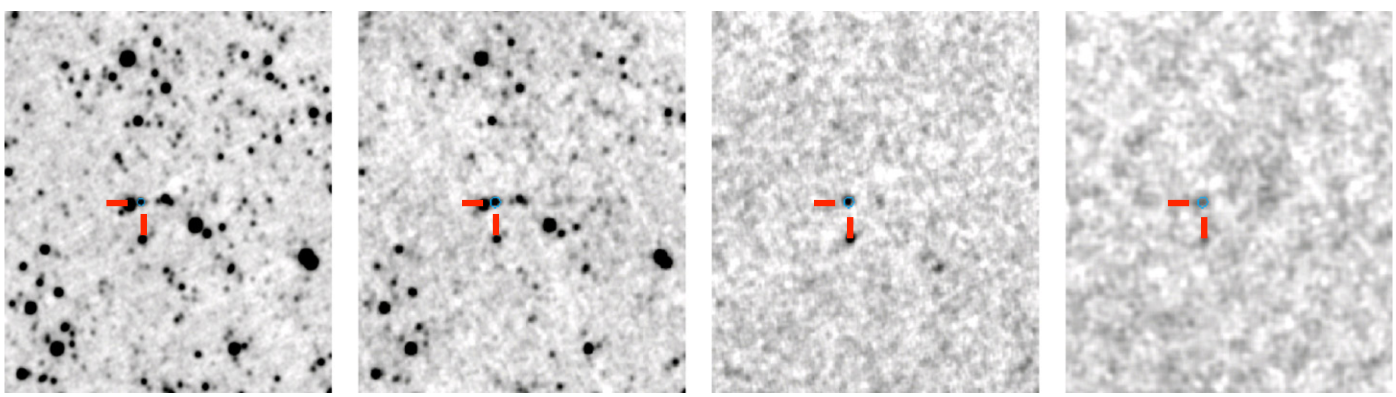

**Figure 12.** *WISE W*1 to *W*4 images, from left to right, of object C.

In studies of cluster membership, some researchers would assign a membership probability for each star, considering its location relative to the cluster center, proper motions, radial velocity, etc., and decide on a threshold probability for membership. As such, the probabilistic nature has to be taken into account when the total mass and the luminosity function are derived, e.g., a candidate with an 80% probability should have its mass weighted by 0.8 and be counted as 0.8 stars. The uncertainty arises, then, if a 0.8 star is really worth twice as much as a 0.4 star in derivation of cluster parameters. In contrast, our analysis exploits a control field to remove sample contaminations. The likelihood of a star being a member of the cluster region depends on the number of false positives in the control field. As seen in Figure 8, our member list is highly reliable for almost the entire bright sample, i.e., for candidates more massive than $\sim$0.1–0.2 $M_\odot$ ($J \lesssim 13$ mag), with only a few false positives.

#### 4.3.1. Luminosity Function and Mass Function

The cluster's $J$-band luminosity function is depicted in Figure 16. For the bright members, the luminosity function has been derived by subtraction of the $J$-magnitude distribution toward the cluster region by that toward the control field. The luminosity function at the faint end, lacking a control field, is given as is. This does not affect our result significantly because each of our substellar candidates has been examined spectroscopically, so contamination is expected to be low. Moreover, the unique colors at very low masses, e.g., in $Z-K$ in Figure 9, would result in little field confusion, hence creditable candidacy. The luminosity function derived in this work, therefore, is reliable except for $J = 14$–16 mag, which has not been corrected for field subtraction.

The $J$-band luminosity function of the cluster increases with magnitude up to $J \sim 12$ mag, and falls off rapidly toward fainter magnitudes. In the $K$-band luminosity of Coma Ber

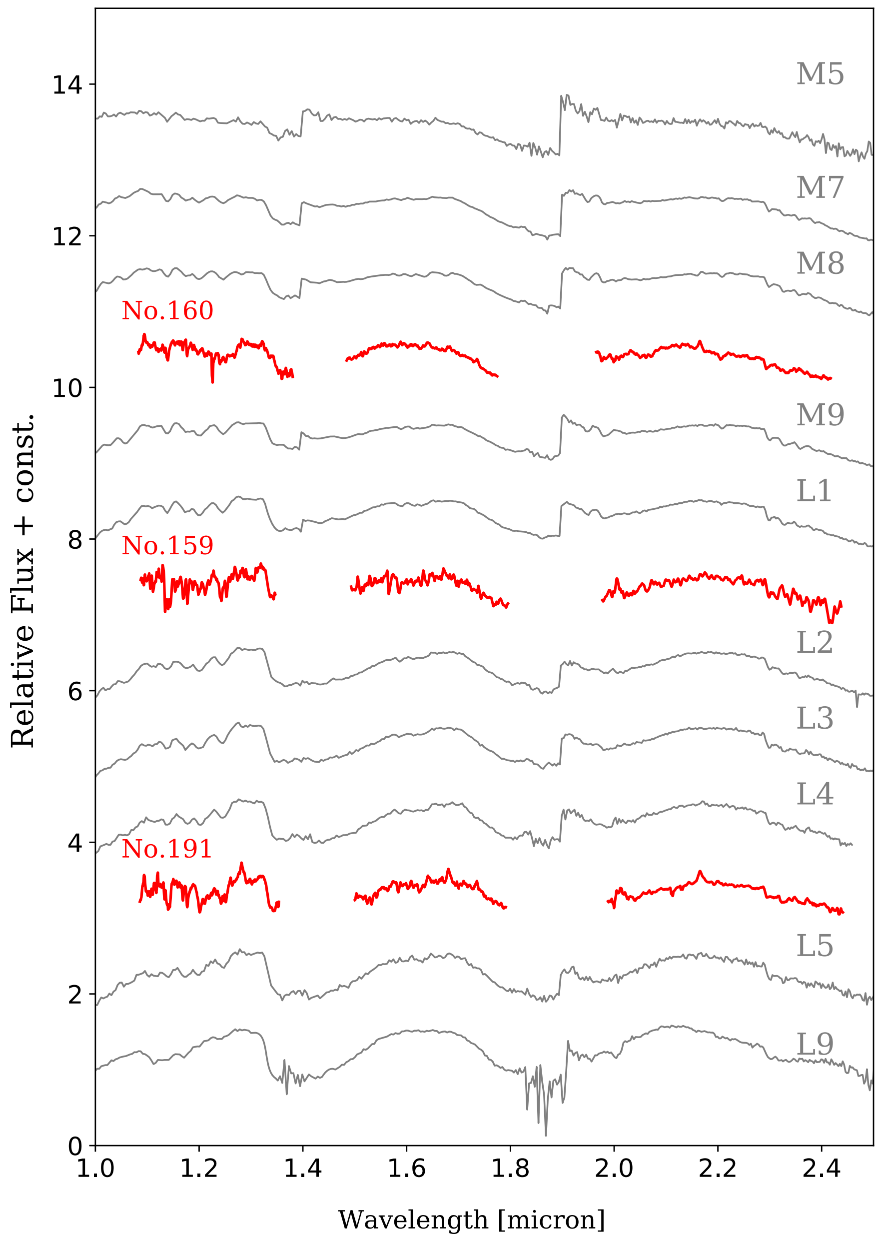


**Figure 13.** Spectra of candidates No. 159, 160, and 191. Also shown are brown dwarf template spectra: M5 (2MASS J01405263+0453302, Kirkpatrick et al. 2010); M7 (VB 8, Burgasser et al. 2008); M8 (VB 10, Burgasser et al. 2004); M9 (LHS2924, Burgasser & McElwain 2006); L1 (2MASSW J2130446−084520, Kirkpatrick et al. 2010); L2 (Kelu-1, Burgasser et al. 2007); L3 (2MASSW J1506544+132106, Burgasser 2007); L4 (2MASS J21580457−1550098, Kirkpatrick et al. 2010); L5 (SDSS J083506.16+195304.4, Chiu et al. 2006); and L9 (DENIS-P J0255−4700, Burgasser et al. 2006)

derived by Casewell et al. (2006), they found a paucity around $K \sim 8$–12 mag, but otherwise no difference fainter than $K \sim 12$ mag between the cluster and a controlled sample chosen by proper motions. Our results show no such shortfall.

The present-day mass function of Coma Ber is exhibited in Figure 17. We convert from the $J$ magnitude to mass according to PARSEC, or, toward the fainter magnitudes, the AMES-Dusty model, based on the cluster luminosity function shown in Figure 16(b). The number of members increases in general from high toward low masses until about $0.3\,M_{\odot}$, a phenomenon commonly seen in star clusters or associations (Bastian et al. 2010). A linear least-squares fit gives a slope, in the sense of $dN/dm = m^{-\alpha}$, $\alpha \approx 0.49 \pm 0.03$, if the two most massive bins for post-main-sequence objects with uncertain masses are excluded. This is close to the value reported by Kraus & Hillenbrand (2007) $\alpha = 0.6 \pm 0.3$ for 0.1–1 $M_{\odot}$, but much shallower than either the nominal Salpeter $\alpha = 2.35$ initial mass function in the solar neighborhood for 1–10 $M_{\odot}$, the present-day mass function of field M dwarfs $\alpha \approx 1.3$ for 0.1–0.7 $M_{\odot}$ (Reid et al. 2002), or, in nearby young star clusters or associations, $\alpha \approx 1.3\ M_{\odot}$ (Hillenbrand & White 2004).

Currently the statistics of the substellar population in star clusters are poorly constrained; less than a handful of stellar systems have been surveyed comprehensively, and even these may be subject to contamination. Furthermore, the age dependence (hence model dependence) of the spectral type with mass hampers derivation of a reliable substellar mass function. Melnikov & Eislöffel (2012) derived a mass function with $\alpha \approx 0.6$ from $0.2\,M_{\odot}$ to $0.14\,M_{\odot}$, and $\alpha \approx 0$ toward lower-masses from $0.14\,M_{\odot}$ to $0.06\,M_{\odot}$. The sky area of their analysis,

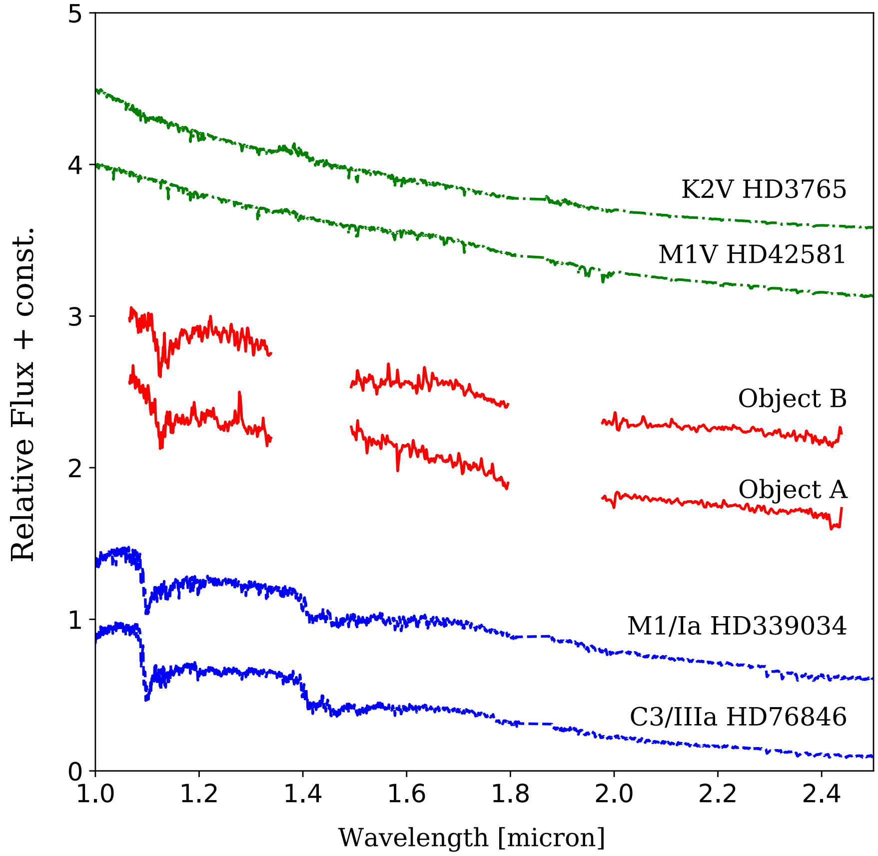


**Figure 14.** Spectra of objects A and B, and template spectra of cool stars (Rayner et al. 2009). Both show the CN feature near 1.1 $\mu$m that is also seen in the giant and supergiant spectra.

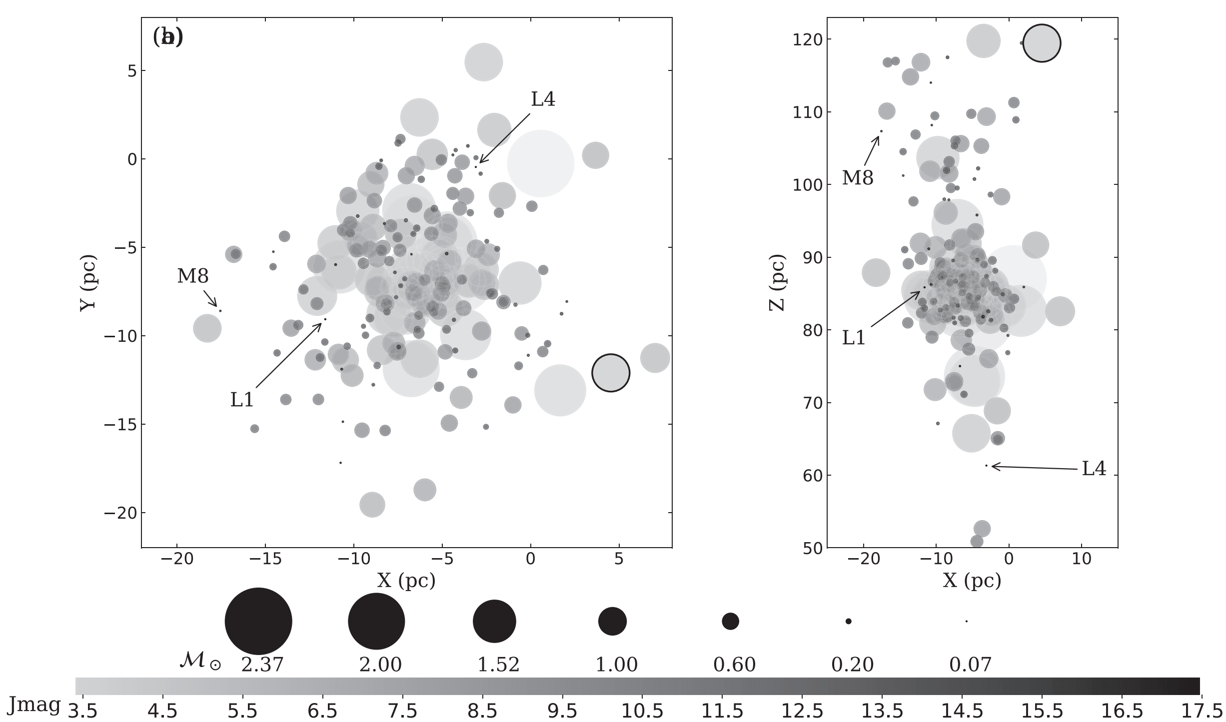


**Figure 15.** The spatial distribution of member candidates in the Galactic (a) $X$–$Y$ coordinates, and (b) $X$–$Z$ coordinates. The size and shade of the circle symbol represent the mass and the $J$ mag, respectively. The three spectroscopically confirmed brown dwarfs reported here are labeled. The one encircled with a dark boundary marks HD 109390, a member proposed by Kraus & Hillenbrand (2007), but with a distance marginally outside our selection range (see Table 3).

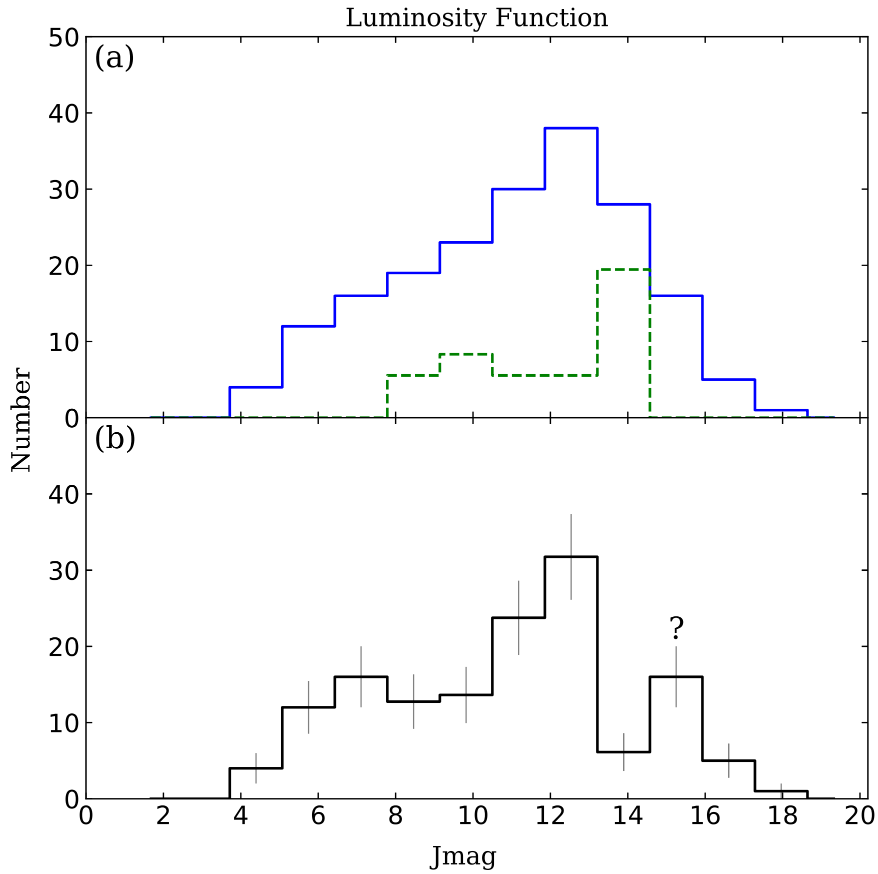


**Figure 16.** (a) $J$-band magnitude distributions toward the cluster region (histogram in solid lines) and toward the control field (in dashed lines). No control field is available for the faint sample. (b) The cluster's luminosity function. It is derived after field subtraction for the bright sample. For $J = 14$–16 mag, it is uncertain, and thus annotated by a question mark, because of no field subtraction. Fainter than $\sim J = 16$ mag, field confusion is low, so the luminosity function is expected to be reliable.

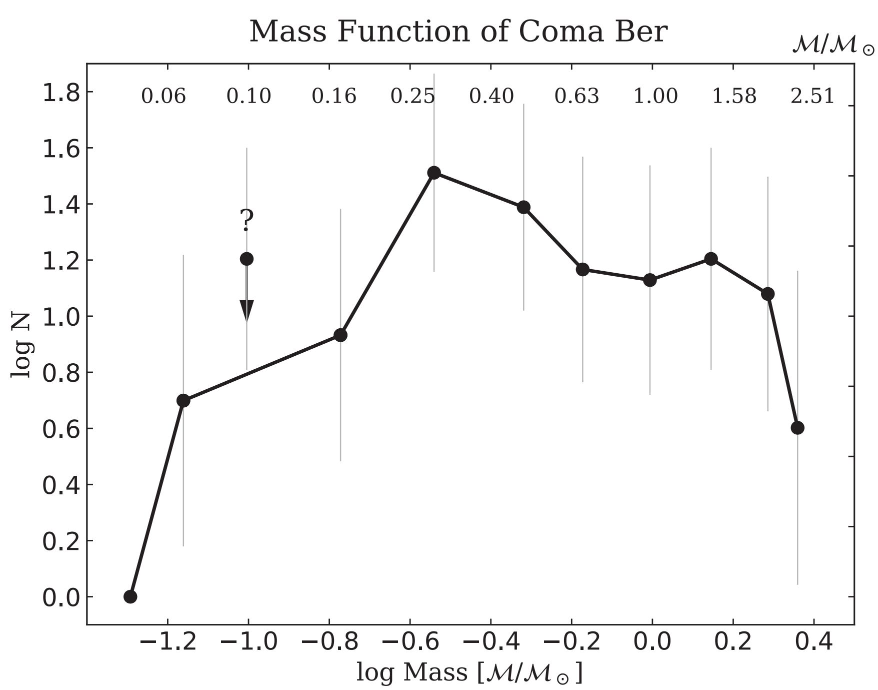


**Figure 17.** The mass function derived by the cluster's $J$-band luminosity function exhibited in Figure 16(b), with mass estimated by the PARSEC or Dusty models. The data point around 0.1 $M_\odot$, considered unreliable because of the uncertainty in the corresponding luminosity function, is labeled by a question mark.

$\sim 2\overset{\circ}{.}7$ in radius, however, covered only part of the core of the cluster. Moreover, lacking a control sample, their member list could be considerably polluted. Among the five photometric brown dwarf candidates these authors proposed (their Table 2), F9 −1134 is not detected by UKIDSS/GCS; C3−250 satisfies the proper motion criterion, but has an inconsistent $Z - K$ color; both D3−1251, with $(\mu_\alpha \cos\delta \approx \mu_\delta) \approx -130$ mas yr$^{-1}$, and G1 −3083, with $(\mu_\alpha \cos\delta, \mu_\delta) \approx (-100, -79)$ mas yr$^{-1}$, have too large proper motions as members. Only E3−5219 turns out to be an M9 member (Casewell et al. 2005, 2014), and also was recovered by us (No. 176).

For our sample, the mass function below 0.3 $M_\odot$ declines monotonically with decreasing mass, and continues into the substellar regime, with a slope $\alpha = -1.69 \pm 0.14$, if the anomaly near 0.1 $M_\odot$ corresponding to the unreliable bin in the luminosity function, is excluded. This contrasts with the flat slope that Kraus & Hillenbrand (2007) found in Coma Ber, or Goldman et al. (2013) derived in Hyades, which is also an intermediate-age cluster (650 Myr Perryman et al. 1998). The slopes at the low masses have been found even to be positive in some very young star clusters (a few Mys), e.g., $\alpha = 0.3$–0.8 for $\lambda$ Orionis (Bayo et al. 2011), or $\alpha \sim 0.5$ for $\rho$ Ophiuchi (Luhman & Rieke 1999; Bastian et al. 2010). However, as we learn in our study, recognition of true members is susceptible to field confusion. The situation must be escalated in star-forming regions where dust extinction, often variable, becomes excessive.

#### *4.3.2. Dynamical Status*

In terms of the number of members, Coma Ber is definitely underpopulated. As presented above, of the 192 candidates we identified, 44 are likely field contaminations, leaving 148 members. On the one hand, there may be faint members in the UKIDSS/GCS void regions that were not found by us. On the other hand, the number of members must decrease if a control sample is available for the faint sample. Artyukhina & Kholopov (1966) estimated a core radius of 2.6 pc and a halo radius of 7 pc, similar to those of the Pleiades and Praesepe, both of similar ages, but Coma Ber contains half the number of members in the core, with a relatively enriched halo population. Adopting the isochrone masses for the post-main-sequence members, the total mass of the 148 members in Coma Ber is $\sim$102 $M_\odot$. This is comparable to what Kraus & Hillenbrand (2007) reported for the 145 members earlier than M6, amounting to a total stellar mass $\sim$112 $M_\odot$, and to the 102 $M_\odot$ estimated by Casewell et al. (2006). Given an effective radius of 10 pc, within which the majority of the members are located, the stellar mass density is 0.024 $M_\odot$ pc$^{-3}$, one order lower than the threshold of 0.1 $M_\odot$ pc$^{-3}$ necessary to remain dynamically stable against tidal disruption in the solar neighborhood (Bok 1934; Lada et al. 1984). With a high Galactic latitude, Coma Ber has an almost null radial velocity (RV), with an RV dispersion $\approx$0.5 km s$^{-1}$ (Odenkirchen et al. 1998). The proper motion data are not accurate enough to estimate the tangential velocity dispersion, but if we assume a space velocity dispersion twice as much as that of the RV, the cluster would have a kinetic energy comparable to the gravitational energy, again suggestive of a marginally bound state. Coma Ber therefore must be disintegrating, as also evidenced by its overall shape stretching along the Galactic motion of the cluster, and with a distribution of comoving, escaped stars that are on average fainter than members in the core and halo (Odenkirchen et al. 1998).

## 5. Summary

We have identified and characterized the stellar and substellar member candidates of the Coma star cluster on the basis of photometry, colors, and proper motions by 2MASS, UKIDSS, and URAT1, plus distance information from *Gaia*/DR2. Out of the 192 candidates found, after field contamination is considered, 148 true members are expected. The candidate list is largely complete within a 5° radius of the cluster, and to our knowledge is the most reliable to date in the literature. We have determined the age of Coma Ber to be about 800 Myr, older than previously adopted. The cluster has a shallower main-sequence mass function than in the field. The mass function peaks around 0.3 $M_\odot$, and decreases rapidly toward the brown dwarf masses. The cluster is mass-segregated, and has a shape elongated toward the Galactic plane, in the process of disintegration. There are nine substellar members, six known to be of late-M types, and we have confirmed their membership. In addition, three brown dwarf members have been spectroscopically confirmed to be an M8, an L1 and an L4, extending from the previously known late-M type for the first time to the mid-L spectral type in this elusive star cluster.

S.Y.T., W.P.C., and P.S.C. acknowledge the financial support of the grants *MOST* 106-2112-M-008-005-MY3 and *MOST* 105-2119-M-008-028-MY3. This research uses data obtained through the Telescope Access Program (TAP), which has been funded by the National Astronomical Observatories of China, the Chinese Academy of Sciences, and the Special Fund for Astronomy from the Ministry of Finance. This study was supported by Sonderforschungsbereich SFB 881 "The Milky Way System" (subproject B7) of the German Research Foundation (DFG). This work has made use of data from the European Space Agency (ESA) mission *Gaia* (https://www.cosmos.esa.int/gaia), processed by the *Gaia* Data Processing and Analysis Consortium (DPAC, https://www.cosmos.esa.int/web/gaia/dpac/consortium). Funding for the DPAC has been provided by national institutions, in particular the institutions participating in the *Gaia* Multilateral Agreement. This research has made use of the 2MASS, SDSS, UKIDSS, *WISE*, PS1 data, as well as the VizieR catalog access tool and the SpeX Prism Spectral Libraries. We thank the anonymous referee, whose constructive suggestions greatly improved the quality of the paper.

## Appendix
## Photometric Spectral Typing and Distance

We have modified the method *photo-type* proposed by Skrzypek et al. (2015, 2016) for spectral typing, which then in turn is used for distance estimation. Skrzypek et al. (2015) included spectral templates from types M5 to T9. To identify cluster members in Coma Ber, we extend to include main-sequence templates. For types from B2 to M4, the median colors and absolute magnitudes are taken from Pecaut et al. (2012) and Pecaut & Mamajek (2013), converting their Johnson colors to the SDSS system by the equations in Jordi et al. (2005). For spectral types later than M7, we adopt the median colors and absolute magnitudes from Best et al. (2018), using the equations in Hewett et al. (2006) to convert between 2MASS and UKIDSS systems. For M dwarfs, we use the median colors from Best et al. (2018) and the absolute magnitudes from Pecaut et al. (2012) and Pecaut & Mamajek (2013). Tables 6–8 list, respectively, these median colors.

**Table 6**
Stellar Colors from B2 to M4

| SpTy | $g - r$ | $r - i$ | $i - z$ | $z - J$ | $J - H$ | $H - K_s$ | $K - W1$ |
|---|---|---|---|---|---|---|---|
| B1.5 | −0.330 | −0.397 | −0.169 | 0.168 | −0.132 | −0.05 | 0.035 |
| B2 | −0.289 | −0.369 | −0.166 | 0.232 | −0.113 | −0.027 | 0.036 |
| B2.5 | −0.277 | −0.357 | −0.167 | 0.266 | −0.105 | −0.025 | 0.036 |
| B3 | −0.259 | −0.347 | −0.166 | 0.289 | −0.098 | −0.022 | 0.036 |
| B4 | −0.246 | −0.338 | −0.166 | 0.305 | −0.092 | −0.018 | 0.036 |
| B5 | −0.238 | −0.331 | −0.166 | 0.326 | −0.089 | −0.021 | 0.036 |
| B6 | −0.222 | −0.320 | −0.164 | 0.348 | −0.081 | −0.009 | 0.035 |
| B7 | −0.211 | −0.313 | −0.165 | 0.368 | −0.077 | −0.003 | 0.035 |
| B8 | −0.192 | −0.299 | −0.163 | 0.395 | −0.067 | 0.007 | 0.034 |
| B9 | −0.153 | −0.273 | −0.157 | 0.449 | −0.05 | 0.02 | 0.032 |
| B9.5 | −0.132 | −0.259 | −0.154 | 0.483 | −0.044 | 0.024 | 0.031 |
| A0 | −0.087 | −0.238 | −0.146 | 0.512 | −0.032 | 0.032 | 0.03 |
| A1 | −0.047 | −0.217 | −0.139 | 0.520 | −0.024 | 0.034 | 0.03 |
| A2 | −0.011 | −0.193 | −0.127 | 0.537 | −0.01 | 0.04 | 0.029 |
| A3 | 0.005 | −0.184 | −0.123 | 0.558 | −0.002 | 0.032 | 0.029 |
| A4 | 0.057 | −0.155 | −0.107 | 0.583 | 0.022 | 0.038 | 0.029 |
| A5 | 0.078 | −0.144 | −0.100 | 0.598 | 0.031 | 0.039 | 0.029 |
| A6 | 0.088 | −0.138 | −0.099 | 0.606 | 0.036 | 0.044 | 0.029 |
| A7 | 0.130 | −0.116 | −0.085 | 0.633 | 0.055 | 0.045 | 0.029 |
| A8 | 0.172 | −0.092 | −0.072 | 0.660 | 0.075 | 0.045 | 0.028 |
| A9 | 0.177 | −0.089 | −0.070 | 0.663 | 0.078 | 0.042 | 0.028 |
| F0 | 0.219 | −0.066 | −0.057 | 0.699 | 0.098 | 0.042 | 0.028 |
| F1 | 0.262 | −0.043 | −0.042 | 0.694 | 0.119 | 0.051 | 0.028 |
| F2 | 0.304 | −0.019 | −0.029 | 0.710 | 0.14 | 0.05 | 0.028 |
| F3 | 0.320 | −0.011 | −0.024 | 0.720 | 0.147 | 0.053 | 0.028 |
| F4 | 0.345 | 0.003 | −0.015 | 0.737 | 0.159 | 0.051 | 0.028 |
| F5 | 0.373 | 0.018 | −0.004 | 0.740 | 0.173 | 0.057 | 0.028 |
| F6 | 0.419 | 0.041 | 0.010 | 0.755 | 0.199 | 0.061 | 0.028 |
| F7 | 0.446 | 0.054 | 0.019 | 0.772 | 0.213 | 0.057 | 0.027 |
| F8 | 0.466 | 0.064 | 0.025 | 0.779 | 0.225 | 0.065 | 0.027 |
| F9 | 0.488 | 0.074 | 0.034 | 0.791 | 0.237 | 0.063 | 0.027 |
| G0 | 0.534 | 0.096 | 0.051 | 0.805 | 0.262 | 0.068 | 0.027 |
| G1 | 0.542 | 0.100 | 0.053 | 0.806 | 0.267 | 0.073 | 0.027 |
| G2 | 0.588 | 0.119 | 0.070 | 0.853 | 0.293 | 0.077 | 0.028 |
| G3 | 0.598 | 0.124 | 0.073 | 0.841 | 0.299 | 0.071 | 0.028 |
| G4 | 0.611 | 0.129 | 0.077 | 0.847 | 0.307 | 0.073 | 0.028 |
| G5 | 0.617 | 0.131 | 0.080 | 0.840 | 0.31 | 0.08 | 0.028 |
| G6 | 0.640 | 0.141 | 0.087 | 0.865 | 0.324 | 0.076 | 0.028 |
| G7 | 0.649 | 0.145 | 0.092 | 0.863 | 0.329 | 0.081 | 0.028 |
| G8 | 0.672 | 0.155 | 0.099 | 0.888 | 0.342 | 0.078 | 0.028 |
| G9 | 0.712 | 0.171 | 0.113 | 0.904 | 0.365 | 0.085 | 0.029 |
| K0 | 0.751 | 0.186 | 0.130 | 0.9189 | 0.387 | 0.093 | 0.03 |
| K1 | 0.781 | 0.199 | 0.139 | 0.835 | 0.402 | 0.098 | 0.03 |
| K2 | 0.832 | 0.222 | 0.164 | 0.966 | 0.432 | 0.098 | 0.031 |
| K3 | 0.934 | 0.266 | 0.209 | 1.024 | 0.49 | 0.11 | 0.034 |
| K4 | 1.074 | 0.344 | 0.284 | 1.051 | 0.544 | 0.126 | 0.039 |
| K5 | 1.139 | 0.384 | 0.315 | 1.067 | 0.568 | 0.132 | 0.042 |
| K6 | 1.250 | 0.459 | 0.357 | 1.105 | 0.601 | 0.149 | 0.049 |
| K7 | 1.351 | 0.539 | 0.374 | 1.174 | 0.622 | 0.168 | 0.06 |
| K8 | 1.384 | 0.578 | 0.371 | 1.211 | 0.623 | 0.177 | 0.081 |
| K9 | 1.417 | 0.617 | 0.368 | 1.237 | 0.625 | 0.185 | 0.101 |
| M0 | 1.451 | 0.657 | 0.365 | 1.284 | 0.626 | 0.194 | 0.122 |
| M0.5 | 1.497 | 0.730 | 0.348 | 1.343 | 0.62 | 0.21 | 0.13 |
| M1 | 1.520 | 0.838 | 0.295 | 1.456 | 0.613 | 0.227 | 0.137 |
| M1.5 | 1.531 | 0.891 | 0.273 | 1.522 | 0.607 | 0.233 | 0.105 |
| M2 | 1.545 | 0.954 | 0.245 | 1.610 | 0.6 | 0.23 | 0.11 |
| M2.5 | 1.568 | 1.055 | 0.208 | 1.818 | 0.589 | 0.151 | 0.117 |
| M3 | 1.591 | 1.1416 | 0.182 | 1.799 | 0.579 | 0.281 | 0.122 |
| M3.5 | 1.650 | 1.339 | 0.141 | 2.049 | 0.558 | 0.272 | 0.132 |
| M4 | 1.702 | 1.454 | 0.126 | 2.175 | 0.557 | 0.283 | 0.139 |

**Note.** Stellar median colors from Pecaut et al. (2012) and Pecaut & Mamajek (2013). Photometric systems are in SDSS, 2MASS, and *WISE*.

**Table 7**
Colors of M Dwarfs

| SpTy | $g - r$ | $r - i$ | $i - z$ | $z - y$ | $y - J$ | $J - H$ | $H - K_s$ | $K_s - W1$ | $W1 - W2$ |
|---|---|---|---|---|---|---|---|---|---|
| M0 | 1.19 | 0.67 | 0.31 | 0.17 | 1.12 | 0.66 | 0.18 | 0.1 | 0.02 |
| M1 | 1.22 | 0.85 | 0.39 | 0.2 | 1.14 | 0.64 | 0.21 | 0.12 | 0.07 |
| M2 | 1.21 | 1.02 | 0.46 | 0.23 | 1.16 | 0.62 | 0.22 | 0.12 | 0.12 |
| M3 | 1.21 | 1.22 | 0.55 | 0.27 | 1.2 | 0.6 | 0.24 | 0.14 | 0.16 |
| M4 | 1.23 | 1.46 | 0.67 | 0.32 | 1.25 | 0.59 | 0.26 | 0.16 | 0.18 |
| M5 | 1.31 | 1.88 | 0.87 | 0.44 | 1.34 | 0.59 | 0.31 | 0.19 | 0.21 |
| M6 | 1.33 | 2.13 | 0.98 | 0.51 | 1.4 | 0.6 | 0.33 | 0.21 | 0.22 |
| M7 | 1.4 | 2.55 | 1.2 | 0.67 | 1.54 | 0.63 | 0.39 | 0.22 | 0.23 |
| M8 | 1.53 | 2.7 | 1.38 | 0.81 | 1.66 | 0.68 | 0.43 | 0.26 | 0.23 |
| M9 | 1.79 | 2.58 | 1.44 | 0.92 | 1.77 | 0.71 | 0.48 | 0.31 | 0.26 |

**Note.** Stellar median colors of M dwarfs from Best et al. (2018). Photometric systems are in PS1, 2MASS, and *WISE*.

**Table 8**
Median Colors of Brown Dwarfs

| SpTy | $i - z$ | $z - Y$ | $Y - J$ | $J - H$ | $H - K$ | $K - W1$ | $W1 - W2$ |
|---|---|---|---|---|---|---|---|
| M5 | 0.91 | 0.47 | 0.55 | 0.45 | 0.32 | 0.11 | 0.17 |
| M6 | 1.45 | 0.6 | 0.67 | 0.53 | 0.39 | 0.22 | 0.21 |
| M7 | 1.36 | 0.55 | 0.68 | 0.54 | 0.38 | 0.17 | 0.2 |
| M8 | 1.68 | 0.69 | 0.79 | 0.56 | 0.44 | 0.19 | 0.22 |
| M9 | 1.86 | 0.79 | 0.87 | 0.59 | 0.49 | 0.22 | 0.23 |
| L0 | 2.01 | 0.86 | 1.04 | 0.63 | 0.54 | 0.29 | 0.27 |
| L1 | 2.02 | 0.88 | 1.11 | 0.67 | 0.58 | 0.33 | 0.28 |
| L2 | 2.04 | 0.9 | 1.18 | 0.73 | 0.63 | 0.4 | 0.28 |
| L3 | 2.1 | 0.92 | 1.23 | 0.79 | 0.67 | 0.48 | 0.29 |
| L4 | 2.2 | 0.94 | 1.27 | 0.86 | 0.71 | 0.56 | 0.3 |
| L5 | 2.33 | 0.97 | 1.31 | 0.91 | 0.74 | 0.65 | 0.32 |
| L6 | 2.51 | 1.0 | 1.33 | 0.96 | 0.75 | 0.72 | 0.36 |
| L7 | 2.71 | 1.04 | 1.35 | 0.97 | 0.75 | 0.77 | 0.41 |
| L8 | 2.93 | 1.09 | 1.21 | 0.96 | 0.71 | 0.79 | 0.48 |
| L9 | 3.15 | 1.16 | 1.2 | 0.9 | 0.65 | 0.79 | 0.57 |
| T0 | 3.36 | 1.23 | 1.19 | 0.8 | 0.56 | 0.76 | 0.68 |
| T1 | 3.55 | 1.33 | 1.19 | 0.65 | 0.45 | 0.71 | 0.82 |
| T2 | 3.7 | 1.43 | 1.18 | 0.46 | 0.31 | 0.65 | 0.99 |
| T3 | 3.82 | 1.55 | 1.18 | 0.25 | 0.16 | 0.59 | 1.19 |
| T4 | 3.9 | 1.68 | 1.17 | 0.02 | 0.01 | 0.55 | 1.43 |
| T5 | 3.95 | 1.81 | 1.16 | −0.19 | −0.11 | 0.54 | 1.7 |
| T6 | 3.98 | 1.96 | 1.16 | −0.35 | −0.19 | 0.59 | 2.02 |
| T7 | 4.01 | 2.11 | 1.15 | −0.43 | −0.2 | 0.7 | 2.38 |
| T8 | 4.08 | 2.26 | 1.15 | −0.36 | −0.09 | 0.9 | 2.79 |

**Note.** Stellar median colors of brown dwarfs from Skrzypek et al. (2015) and Skrzypek et al. (2016) Photometric systems are in SDSS (Vega), UKIDSS, and *WISE*.

The algorithm performs classification by finding the minimum $\chi^2$ among spectral templates. Given an object with photometry $m_b$ ($b = g, r, i \ldots W2$), we define the "reference" magnitude, $m_{(B,t)}$, at the band $B$ ($B = J$ band, in this study) for each spectral type $t$ by,

$$m_{(B,t)} = \frac{\sum_{b=1}^{N_b} \frac{m_b - c_{(b,t)}}{\sigma_b^2}}{\sum_{b=1}^{N_b} \frac{1}{\sigma_b^2}}, \tag{1}$$

where the parameters $c_{(b,t)}$ are the expected colors of each spectral type $t$ listed in Tables 6–8. The $m_{(B,t)}$ could be regarded as the pseudo-$J$ magnitude for the $t$ spectral type.

Next, the weighted $\chi^2$ is derived:

$$\chi^2(\{m_b\}, \{\sigma_b\}, m_{(B,t)}, t) = \sum_{b=1}^{N_b} \left( \frac{m_b - m_{(B,t)} - c_{(b,t)}}{\sigma_b} \right)^2. \tag{2}$$

For each spectral type $t$, $m_b - m_{(B,t)}$ is the "observed" value, while $c_{(b,t)}$ is the expectation. Finally, the spectral type with the minimum $\chi^2$ among all templates is considered the best-fit type for the target. Figure 18 shows a general consistency with $\pm 2$ subtypes between the *photo-type* results and those measured by SDSS/DR14. Once the spectral type is determined, the absolute magnitudes listed in Table 9 are used to estimate the distance for each band. The median value of all bands is thereby adopted as the distance to the object.

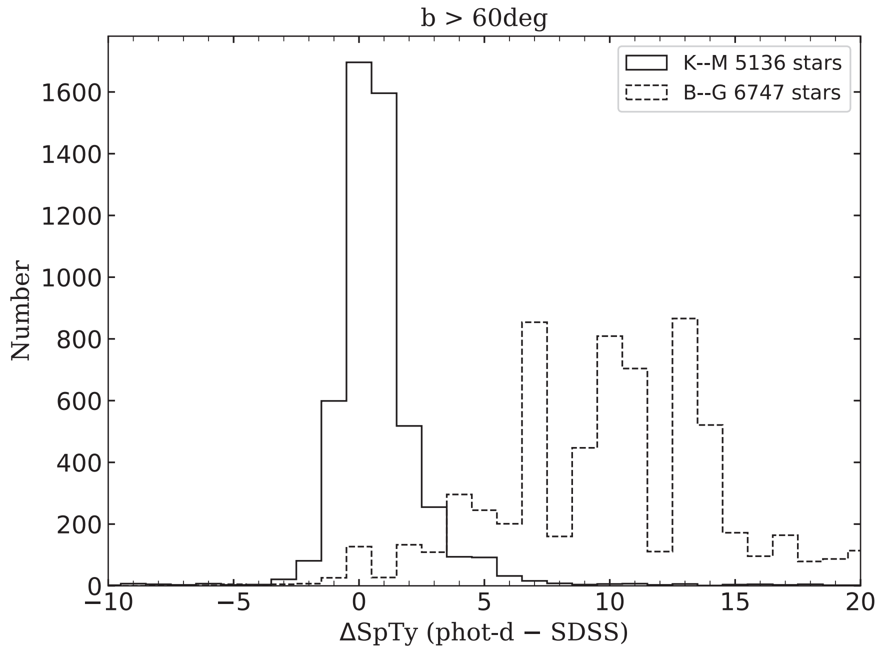


**Figure 18.** Differences between *phot-d* estimated spectral types and SDSS observed spectral types for K and M (solid lines) and for B–G dwarfs (dashed lines). Only stars above the Galactic latitude 60° have been selected, to minimize the effect of interstellar reddening.

**Table 9**
Absolute Magnitudes

| SpTy | $g$ | $r$ | $i$ | $z$ | $y$ | $J$ | $H$ | $K_s$ | $W1$ | $W2$ |
|---|---|---|---|---|---|---|---|---|---|---|
| B1.5 | −2.959 | −2.628 | −2.231 | −2.062 | ⋯ | −2.23 | −2.098 | −2.05 | −2.085 | ⋯ |
| B2 | −1.832 | −1.543 | −1.175 | −1.008 | ⋯ | −1.24 | −1.127 | −1.1 | −1.136 | ⋯ |
| B2.5 | −1.525 | −1.248 | −0.891 | −0.724 | ⋯ | −0.99 | −0.885 | −0.86 | −0.896 | ⋯ |
| B3 | −1.212 | −0.953 | −0.607 | −0.441 | ⋯ | −0.73 | −0.632 | −0.61 | −0.646 | ⋯ |
| B4 | −1.104 | −0.858 | −0.520 | −0.355 | ⋯ | −0.66 | −0.568 | −0.55 | −0.586 | ⋯ |
| B5 | −0.999 | −0.761 | −0.429 | −0.264 | ⋯ | −0.59 | −0.501 | −0.48 | −0.516 | −0.471 |
| B6 | −0.588 | −0.367 | −0.047 | 0.118 | ⋯ | −0.23 | −0.149 | −0.14 | −0.175 | −0.13 |
| B7 | −0.481 | −0.269 | 0.043 | 0.208 | ⋯ | −0.16 | −0.083 | −0.08 | −0.115 | −0.07 |
| B8 | −0.269 | −0.077 | 0.222 | 0.385 | ⋯ | −0.01 | 0.057 | 0.05 | 0.016 | 0.062 |
| B9 | 0.656 | 0.809 | 1.082 | 1.239 | ⋯ | 0.79 | 0.84 | 0.82 | 0.788 | 0.851 |
| B9.5 | 0.769 | 0.900 | 1.160 | 1.313 | ⋯ | 0.83 | 0.874 | 0.85 | 0.819 | 0.863 |
| A0 | 1.11 | 1.197 | 1.436 | 1.582 | ⋯ | 1.07 | 1.102 | 1.07 | 1.04 | 1.081 |
| A1 | 1.367 | 1.414 | 1.631 | 1.780 | ⋯ | 1.25 | 1.274 | 1.24 | 1.21 | 1.246 |
| A2 | 1.527 | 1.537 | 1.730 | 1.857 | ⋯ | 1.32 | 1.33 | 1.29 | 1.261 | 1.295 |
| A3 | 1.607 | 1.601 | 1.785 | 1.908 | ⋯ | 1.35 | 1.352 | 1.32 | 1.291 | 1.324 |
| A4 | 1.848 | 1.791 | 1.946 | 2.053 | ⋯ | 1.47 | 1.448 | 1.41 | 1.381 | 1.412 |
| A5 | 1.941 | 1.863 | 2.007 | 2.108 | ⋯ | 1.51 | 1.479 | 1.44 | 1.411 | 1.441 |
| A6 | 1.997 | 1.909 | 2.047 | 2.146 | ⋯ | 1.54 | 1.504 | 1.46 | 1.431 | 1.461 |
| A7 | 2.202 | 2.072 | 2.188 | 2.273 | ⋯ | 1.64 | 1.585 | 1.54 | 1.511 | 1.541 |
| A8 | 2.448 | 2.275 | 2.368 | 2.440 | ⋯ | 1.78 | 1.705 | 1.66 | 1.632 | 1.66 |
| A9 | 2.461 | 2.283 | 2.372 | 2.443 | ⋯ | 1.78 | 1.702 | 1.66 | 1.632 | 1.66 |
| F0 | 2.695 | 2.476 | 2.543 | 2.599 | ⋯ | 1.90 | 1.802 | 1.76 | 1.732 | 1.758 |
| F1 | 3.000 | 2.739 | 2.782 | 2.824 | ⋯ | 2.13 | 2.011 | 1.96 | 1.932 | 1.958 |
| F2 | 3.226 | 2.922 | 2.941 | 2.970 | ⋯ | 2.26 | 2.12 | 2.07 | 2.042 | 2.069 |
| F3 | 3.325 | 3.005 | 3.016 | 3.040 | ⋯ | 2.32 | 2.173 | 2.12 | 2.092 | 2.12 |
| F4 | 3.490 | 3.145 | 3.142 | 3.157 | ⋯ | 2.42 | 2.261 | 2.21 | 2.182 | 2.211 |
| F5 | 3.676 | 3.303 | 3.286 | 3.290 | ⋯ | 2.55 | 2.377 | 2.32 | 2.292 | 2.322 |
| F6 | 4.005 | 3.586 | 3.544 | 3.535 | ⋯ | 2.78 | 2.581 | 2.52 | 2.492 | 2.525 |
| F7 | 4.191 | 3.745 | 3.691 | 3.672 | ⋯ | 2.90 | 2.687 | 2.63 | 2.603 | 2.639 |
| F8 | 4.344 | 3.878 | 3.814 | 3.789 | ⋯ | 3.01 | 2.785 | 2.72 | 2.693 | 2.732 |
| F9 | 4.498 | 4.009 | 3.935 | 3.901 | ⋯ | 3.11 | 2.873 | 2.81 | 2.783 | 2.824 |
| G0 | 4.825 | 4.292 | 4.196 | 4.145 | ⋯ | 3.34 | 3.078 | 3.01 | 2.983 | 3.026 |
| G1 | 4.881 | 4.339 | 4.239 | 4.186 | ⋯ | 3.38 | 3.113 | 3.04 | 3.013 | 3.057 |
| G2 | 5.200 | 4.612 | 4.492 | 4.423 | ⋯ | 3.57 | 3.277 | 3.2 | 3.172 | 3.222 |
| G3 | 5.276 | 4.678 | 4.554 | 4.481 | ⋯ | 3.64 | 3.341 | 3.27 | 3.242 | 3.292 |
| G4 | 5.365 | 4.754 | 4.625 | 4.547 | ⋯ | 3.70 | 3.393 | 3.32 | 3.292 | 3.344 |

**Table 9**
(Continued)

| SpTy | $g$ | $r$ | $i$ | $z$ | $y$ | $J$ | $H$ | $K_s$ | $W1$ | $W2$ |
|---|---|---|---|---|---|---|---|---|---|---|
| G5 | 5.408 | 4.792 | 4.660 | 4.580 | ⋯ | 3.74 | 3.43 | 3.35 | 3.322 | 3.374 |
| G6 | 5.574 | 4.934 | 4.792 | 4.705 | ⋯ | 3.84 | 3.516 | 3.44 | 3.412 | 3.465 |
| G7 | 5.629 | 4.980 | 4.835 | 4.743 | ⋯ | 3.88 | 3.551 | 3.47 | 3.442 | 3.496 |
| G8 | 5.784 | 5.112 | 4.957 | 4.858 | ⋯ | 3.97 | 3.628 | 3.55 | 3.522 | 3.579 |
| G9 | 6.040 | 5.328 | 5.157 | 5.044 | ⋯ | 4.14 | 3.775 | 3.69 | 3.661 | 3.721 |
| K0 | 6.274 | 5.523 | 5.337 | 5.208 | ⋯ | 4.29 | 3.903 | 3.81 | 3.78 | 3.843 |
| K1 | 6.424 | 5.643 | 5.444 | 5.305 | ⋯ | 4.47 | 4.068 | 3.97 | 3.94 | 4.004 |
| K2 | 6.753 | 5.921 | 5.699 | 5.536 | ⋯ | 4.57 | 4.138 | 4.04 | 4.009 | 4.077 |
| K3 | 7.194 | 6.259 | 5.993 | 5.784 | ⋯ | 4.76 | 4.27 | 4.16 | 4.126 | 4.197 |
| K4 | 7.733 | 6.659 | 6.314 | 6.031 | ⋯ | 4.98 | 4.436 | 4.31 | 4.271 | 4.344 |
| K5 | 8.085 | 6.946 | 6.562 | 6.247 | ⋯ | 5.18 | 4.612 | 4.48 | 4.438 | 4.511 |
| K6 | 8.581 | 7.332 | 6.872 | 6.515 | ⋯ | 5.41 | 4.809 | 4.66 | 4.611 | ⋯ |
| K7 | 9.088 | 7.737 | 7.198 | 6.824 | ⋯ | 5.65 | 5.028 | 4.86 | 4.8 | ⋯ |
| K8 | 9.324 | 7.940 | 7.362 | 6.991 | ⋯ | 5.78 | 5.157 | 4.98 | 4.899 | ⋯ |
| K9 | 9.561 | 8.143 | 7.526 | 7.157 | ⋯ | 5.92 | 5.295 | 5.11 | 5.009 | ⋯ |
| M0 | 9.797 | 8.346 | 7.690 | 7.324 | ⋯ | 6.04 | 5.414 | 5.22 | 5.098 | ⋯ |
| M1 | 10.619 | 9.099 | 8.261 | 7.966 | ⋯ | 6.51 | 5.897 | 5.67 | 5.533 | ⋯ |
| M2 | 11.245 | 9.700 | 8.745 | 8.500 | ⋯ | 6.89 | 6.29 | 6.06 | 5.95 | ⋯ |
| M3 | 12.113 | 10.522 | 9.380 | 9.199 | ⋯ | 7.40 | 6.821 | 6.54 | 6.418 | ⋯ |
| M4 | 13.846 | 12.145 | 10.691 | 10.565 | ⋯ | 8.39 | 7.833 | 7.55 | 7.411 | ⋯ |
| M5 | 15.481 | 13.597 | 11.804 | 11.693 | ⋯ | 9.25 | 8.67 | 8.36 | ⋯ | ⋯ |
| M6 | 17.880 | 15.802 | 13.357 | 13.099 | 10.28 | ⋯ | 9.675 | 9.32 | ⋯ | ⋯ |
| M7 | 18.11 | 16.75 | 14.18 | 12.97 | 12.31 | 10.77 | 10.14 | 9.75 | 9.52 | 9.3 |
| M8 | 19.19 | 17.73 | 14.98 | 13.59 | 12.8 | 11.14 | 10.46 | 10.02 | 9.77 | 9.54 |
| M9 | 19.95 | 18.15 | 15.63 | 14.19 | 13.25 | 11.48 | 10.77 | 10.29 | 9.96 | 9.7 |
| L0 | 20.41 | 18.42 | 16.05 | 14.58 | 13.63 | 11.81 | 11.05 | 10.57 | 10.27 | 9.99 |
| L1 | 20.86 | 18.75 | 16.42 | 14.94 | 13.97 | 12.04 | 11.24 | 10.72 | 10.37 | 10.12 |
| L2 | 21.24 | 19.02 | 16.73 | 15.31 | 14.33 | 12.32 | 11.41 | 10.83 | 10.41 | 10.14 |
| L3 | ⋯ | 19.71 | 17.52 | 16.01 | 15.02 | 12.89 | 11.94 | 11.3 | 10.78 | 10.51 |
| L4 | ⋯ | 20.46 | 18.25 | 16.56 | 15.56 | 13.41 | 12.35 | 11.77 | 11.07 | 10.75 |
| L5 | ⋯ | 20.66 | 18.74 | 16.94 | 15.87 | 13.7 | 12.65 | 12.03 | 11.28 | 10.98 |
| L6 | ⋯ | 21.2 | 19.26 | 17.34 | 16.26 | 14.17 | 13.18 | 12.54 | 11.84 | 11.48 |
| L7 | ⋯ | ⋯ | 20.11 | 18.2 | 17.14 | 14.95 | 13.79 | 13.08 | 12.39 | 12.0 |
| L8 | ⋯ | 22.88 | 20.44 | 18.1 | 17.03 | 14.9 | 13.77 | 13.08 | 12.22 | 11.73 |
| L9 | ⋯ | ⋯ | 20.64 | 18.16 | 17.03 | 14.93 | 13.86 | 13.27 | 12.42 | 11.94 |
| T0 | ⋯ | ⋯ | 20.22 | 17.99 | 16.76 | 14.56 | 13.63 | 13.11 | 12.49 | 11.94 |
| T1 | ⋯ | ⋯ | 21.03 | 18.87 | 17.44 | 15.25 | 14.37 | 14.07 | 13.44 | 12.69 |
| T2 | ⋯ | ⋯ | 21.51 | 18.28 | 16.79 | 14.56 | 13.76 | 13.49 | 12.96 | 12.07 |
| T3 | ⋯ | ⋯ | ⋯ | 18.0 | 16.46 | 14.19 | 13.6 | 13.37 | 12.71 | 11.64 |
| T4 | ⋯ | ⋯ | ⋯ | 18.07 | 16.37 | 13.94 | 13.62 | 13.56 | 13.36 | 11.93 |
| T5 | ⋯ | ⋯ | 22.69 | 19.2 | 17.43 | 14.94 | 14.75 | 14.77 | 14.46 | 12.69 |
| T6 | ⋯ | ⋯ | ⋯ | 19.82 | 18.07 | 15.53 | 15.48 | 15.37 | 15.08 | 13.02 |
| T7 | ⋯ | ⋯ | ⋯ | 21.14 | 19.33 | 16.78 | 16.7 | 16.7 | 16.25 | 14.04 |
| T8 | ⋯ | ⋯ | ⋯ | 21.52 | 19.75 | 17.18 | 17.09 | ⋯ | 16.45 | 13.77 |
| T9 | ⋯ | ⋯ | ⋯ | 21.82 | 20.37 | 17.75 | 17.51 | ⋯ | 16.7 | 13.81 |

**Note.** Absolute magnitudes of spectral types. Types earlier than M6 are from Pecaut et al. (2012) and Pecaut & Mamajek (2013) in SDSS, 2MASS, and *WISE* systems. Types M7 and later are from Best et al. (2018) in PS1, 2MASS, and *WISE*.

## ORCID iDs

Shih-Yun Tang https://orcid.org/0000-0003-4247-1401
W. P. Chen https://orcid.org/0000-0003-0262-272X
P. S. Chiang https://orcid.org/0000-0003-3167-2523
Gregory J. Herczeg https://orcid.org/0000-0002-7154-6065

## References

Abt, H. 2008, ApJS, 176, 216
Alam, S., Albareti, F. D., Allende Prieto, C., et al. 2015, ApJS, 219, 12
Argue, A. N., & Kenworthy, C. M. 1969, MNRAS, 146, 479
Artyukhina, N. M., & Kholopov, P. N. 1966, SvA, 10, 448
Bastian, N., Covey, K. R., & Meyer, M. R. 2010, ARA&A, 48, 339
Bayo, A., Barrado, D., Stauffer, J., et al. 2011, A&A, 536, A63
Best, W. M. J., Magnier, E. A., Liu, M. C., et al. 2018, ApJS, 234, 1
Bhattacharya, S., Mishra, I., Vaidya, K., & Chen, W. P. 2017, ApJ, 847, 138
Binney, J., & Tremaine, S. 1987, Galactic Dynamics (Princeton, NJ: Princeton Univ. Press)
Bok, B. J. 1934, HarCi, 384, 1
Boudreault, S., Lodieu, N., Deacon, N. R., & Hambly, N. C. 2012, MNRAS, 426, 3419
Brandner, W., Clark, J. S., Stolte, A., et al. 2008, A&A, 478, 137
Bressan, A., Marigo, P., Girardi, L., et al. 2012, MNRAS, 427, 127
Burgasser, A. J. 2007, ApJ, 659, 655
Burgasser, A. J., Geballe, T. R., Leggett, S. K., Kirkpatrick, J. D., & Golimowski, D. A. 2006, ApJ, 637, 1067
Burgasser, A. J., Liu, M. C., Ireland, M. J., Cruz, K. L., & Dupuy, T. J. 2008, ApJ, 681, 579
Burgasser, A. J., Looper, D. L., Kirkpatrick, J. D., & Liu, M. C. 2007, ApJ, 658, 557

Burgasser, A. J., & McElwain, M. W. 2006, AJ, 131, 1007
Burgasser, A. J., McElwain, M. W., Kirkpatrick, J. D., et al. 2004, AJ, 127, 2856
Casewell, S. L., Jameson, R. F., & Dobbie, P. D. 2005, AN, 326, 991
Casewell, S. L., Jameson, R. F., & Dobbie, P. D. 2006, MNRAS, 365, 447
Casewell, S. L., Littlefair, S. P., Burleigh, M. R., & Roy, M. 2014, MNRAS, 441, 2644
Cayrel de Strobel, G. 1990, MmSAI, 61, 613
Chambers, K. C., Magnier, E. A., Metcalfe, N., et al. 2016, arXiv:1612.05560
Chen, C. W., & Chen, W. P. 2010, ApJ, 721, 1790
Chen, W. P., Chen, C. W., & Shu, C. G. 2004, AJ, 128, 2306
Chen, Y., Bressan, A., Girardi, L., et al. 2015, MNRAS, 452, 1068
Chen, Y., Girardi, L., Bressan, A., et al. 2014, MNRAS, 444, 2525
Chiu, K., Fan, X., Leggett, S. K., et al. 2006, AJ, 131, 2722
Collins, R., & Hambly, N. 2012, in ASP Conf. 461, Astronomical Data Analysis Software and Systems XXI, ed. P. Ballester, D. Egret, & N. P. F. Lorente (San Francisco, CA: ASP), 525
Cox, A. N. 2000, Allen's Astrophysical Quantities (4th ed.; New York: AIP)
Cushing, M. C., Vacca, W. D., & Rayner, J. T. 2004, PASP, 116, 362
Cutri, R. M., Wright, E. L., Conrow, T., et al. 2013, Explanatory Supplement to the AllWISE Data Release Products, http://wise2.ipac.caltech.edu/docs/release/allwise/expsup/
de Grijs, R. 2009, Ap&SS, 324, 283
de Grijs, R., & Parmentier, G. 2007, ChJAA, 7, 155
Ducati, J. R. 2002, yCat, 2237, 1
Elias, J. H., Joyce, R. R., Liang, M., et al. 2006a, Proc. SPIE, 6269, 62694C
Elias, J. H., Rodgers, B., Joyce, R. R., et al. 2006b, Proc. SPIE, 6269, 626914
Ford, A., Jeffries, R. D., James, D. J., & Barnes, J. R. 2001, A&A, 369, 871
Friel, E. D., & Boesgaard, A. M. 1992, ApJ, 387, 170
Gaia Collaboration, van Leeuwen, F., Vallenari, A., et al. 2017, A&A, 601, A19
Gaia Collaboration, Brown, A. G. A., Vallenari, A., et al. 2018, arXiv:1804.09365
Gáspár, A., Rieke, G. H., Su, K. Y. L., et al. 2009, ApJ, 697, 1578
Gennaro, M., Brandner, W., Stolte, A., & Henning, T. 2011, MNRAS, 412, 2469
Goldman, B., Röser, S., Schilbach, E., et al. 2013, A&A, 559, A43
Gratton, R. 2000, in ASP Conf. Ser. 198, Stellar Clusters and Associations: Convection, Rotation, and Dynamos, ed. R. Pallavicini, G. Micela, & S. Sciortino (San Francisco, CA: ASP), 225
Griffin, R., & Griffin, R. 1986, JApA, 7, 195
Griffin, R. E. M., & Griffin, R. F. 2011, AN, 332, 105
Herter, T. L., Henderson, C. P., Wilson, J. C., et al. 2008, Proc. SPIE, 7014, 70140X
Hewett, P. C., Warren, S. J., Leggett, S. K., & Hodgkin, S. T. 2006, MNRAS, 367, 454
Hillenbrand, L. A. 1997, AJ, 113, 1733
Hillenbrand, L. A., & White, R. J. 2004, ApJ, 604, 741
Jeffries, R. D. 1999, MNRAS, 304, 821
Jordi, K., Grebel, E. K., & Ammon, K. 2005, AN, 326, 657
Kippenhahn, R., Meyer-Hofmeister, E., & Thomas, H. C. 1970, A&A, 5, 155
Kirkpatrick, J. D., Cushing, M. C., Gelino, C. R., et al. 2011, ApJS, 197, 19
Kirkpatrick, J. D., Looper, D. L., Burgasser, A. J., et al. 2010, ApJS, 190, 100
Kraus, A. L., & Hillenbrand, L. A. 2007, AJ, 134, 2340
Lada, C. J., & Lada, E. A. 2003, ARA&A, 41, 57
Lada, C. J., Margulis, M., & Dearborn, D. 1984, ApJ, 285, 141
Lançon, A., Hauschildt, P. H., Ladjal, D., & Mouhcine, M. 2007, A&A, 468, 205
Lawrence, A., Warren, S. J., Almaini, O., et al. 2012, yCat, 2314
Lindegren, L., Hernandez, J., Bombrun, A., et al. 2018, arXiv:1804.09366
Lodieu, N., Deacon, N. R., & Hambly, N. C. 2012, MNRAS, 422, 1495
Loidl, R., Lançon, A., & Jørgensen, U. G. 2001, A&A, 371, 1065
Luhman, K. L. 2012, ARA&A, 50, 65
Luhman, K. L., & Rieke, G. H. 1999, ApJ, 525, 440
Mainzer, A., Bauer, J., Grav, T., et al. 2011, ApJ, 731, 53
Martín, E. L., Lodieu, N., Pavlenko, Y., & Béjar, V. J. S. 2018, ApJ, 856, 40
Massarotti, A., Latham, D., Stefanik, R. P., et al. 2008, AJ, 135, 209
Mathieu, R. D. 1984, ApJ, 284, 643
Melnikov, S., & Eislöffel, J. 2012, A&A, 544, A111
Melotte, P. J. 1915, MmRAS, 60, 175
Mermilliod, J.-C., Grenon, M., & Mayor, M. 2008, A&A, 491, 951
Netopil, M., Paunzen, E., Heiter, U., & Soubiran, C. 2016, A&A, 585, A150
Nicolet, B. 1981, A&A, 104, 185
Odenkirchen, M., Soubiran, C., & Colin, J. 1998, NewA, 3, 583
Pecaut, M. J., & Mamajek, E. E. 2013, ApJS, 208, 9
Pecaut, M. J., Mamajek, E. E., & Bubar, E. J. 2012, ApJ, 746, 154
Perryman, M. A. C., Brown, A. G. A., Lebreton, Y., et al. 1998, A&A, 331, 81
Rayner, J. T., Cushing, M. C., & Vacca, W. D. 2009, ApJS, 185, 289
Rayner, J. T., Toomey, D. W., Onaka, P. M., et al. 2003, PASP, 115, 362
Reid, I. N., Gizis, J. E., & Hawley, S. L. 2002, AJ, 124, 2721
Rochau, B., Brandner, W., Stolte, A., et al. 2010, ApJL, 716, L90
Salpeter, E. E. 1955, ApJ, 121, 161
Scholz, R.-D., Bihain, G., Schnurr, O., et al. 2011, A&A, 532, L5
Shu, F. H. 1982, The Physical Universe (Mill Valley, CA: Univ. Science Books)
Skrutskie, M. F., Cutri, R. M., Stiening, R., et al. 2006, AJ, 131, 1163
Skrzypek, N., Warren, S. J., Faherty, J. K., et al. 2015, A&A, 574, A78
Skrzypek, N., Warren, S. J., & Faherty, J. K. 2016, A&A, 589, A49
Smith, L., Lucas, P. W., Burningham, B., et al. 2014, MNRAS, 437, 3603
Tang, J., Bressan, A., Rosenfield, P., et al. 2014, MNRAS, 445, 4287
Terrien, R. C., Mahadevan, S., Deshpande, R., et al. 2014, ApJ, 782, 61
Trumpler, R. J. 1938, LicOB, 18, 167
Tsvetkov, T. G. 1989, Ap&SS, 151, 47
Upgren, A. R. 1962, AJ, 67, 37
Vacca, W. D., Cushing, M. C., & Rayner, J. T. 2003, PASP, 115, 389
van Leeuwen, F. 1999, A&A, 341, L71
van Leeuwen, F. 2009, A&A, 497, 209
Wang, P. F., Chen, W. P., Lin, C. C., et al. 2014, ApJ, 784, 57
West, A. A., Morgan, D. P., Bochanski, J. J., et al. 2011, AJ, 141, 97
Wright, E. L., Eisenhardt, P. R. M., Mainzer, A. K., et al. 2010, AJ, 140, 1868
Zacharias, N., Finch, C., Subasavage, J., et al. 2015, AJ, 150, 101
Zuckerman, B., & Song, I. , 2004, ARA&A, 42, 685